LETTER

doi:10.1038/nature13961

Nutrient-sensing nuclear receptors coordinate autophagy

Jae Man Lee[1], Martin Wagner[1]†, Rui Xiao[1], Kang Ho Kim[1], Dan Feng[2]†, Mitchell A. Lazar[2] & David D. Moore[1]

Autophagy is an evolutionarily conserved catabolic process that recycles nutrients upon starvation and maintains cellular energy homeostasis[1–3]. Its acute regulation by nutrient-sensing signalling pathways is well described, but its longer-term transcriptional regulation is not. The nuclear receptors peroxisome proliferator-activated receptor-α (PPARα) and farnesoid X receptor (FXR) are activated in the fasted and fed liver, respectively[4,5]. Here we show that both PPARα and FXR regulate hepatic autophagy in mice. Pharmacological activation of PPARα reverses the normal suppression of autophagy in the fed state, inducing autophagic lipid degradation, or lipophagy. This response is lost in PPARα knockout (*Ppara*$^{-/-}$, also known as *Nr1c1*$^{-/-}$) mice, which are partially defective in the induction of autophagy by fasting. Pharmacological activation of the bile acid receptor FXR strongly suppresses the induction of autophagy in the fasting state, and this response is absent in FXR knockout (*Fxr*$^{-/-}$, also known as *Nr1h4*$^{-/-}$) mice, which show a partial defect in suppression of hepatic autophagy in the fed state. PPARα and FXR compete for binding to shared sites in autophagic gene promoters, with opposite transcriptional outputs. These results reveal complementary, interlocking mechanisms for regulation of autophagy by nutrient status.

Overlapping networks govern both acute and longer-term responses to nutrients. In the fasted liver, glucagon induces both rapid glycogen breakdown and transcriptional activation of gluconeogenesis[6]. Nutrient deprivation also acutely regulates nutrient reclamation by autophagy[7–9]. Among several transcription factors that have been linked to the control of autophagy at the transcriptional level, activation of the basic helix-loop-helix transcription factor EB (TFEB) by fasting is the best described[10].

Nutrient-sensing nuclear receptors are key integrators of metabolic responses. PPARα is activated by fatty acids in the fasted state, promoting fatty acid oxidation[4,11,12]. In the fed state, FXR is activated by bile acids returning to the liver along with nutrients, suppressing gluconeogenesis[13]. We proposed that PPARα and FXR would directly regulate autophagy, and initially tested the effect of their pharmacological activation in the mouse hepatocyte cell line AML12 expressing a triple fusion protein of monomeric red fluorescent protein (mRFP), green fluorescent protein (GFP) and the autophagosome marker LC3 (mRFP–GFP–LC3)[14–16]. In autophagosomes, the combination of both RFP and GFP in the triple fusion yields yellow fluorescence, whereas autolysosomal delivery results in red. As expected, the yellow fluorescence in normally cultured cells was converted to red by acute nutrient deprivation (Fig. 1 and Extended Data Fig. 1f). The FXR agonist GW4064 (ref. 17) prevented this process in the nutrient-deprived cells, whereas the PPARα agonist GW7647 (ref. 18) mimicked it in non-starved cells (Fig. 1a and Extended Data Fig. 1f). Extensive cell-based studies of levels of LC3 conjugated to phosphatidylethanolamine (LC3-II) and other indicators of autophagy confirmed that these responses are dose and time dependent, and indicated that they are not dependent on altered mammalian target of rapamycin complex 1 (mTORC1) activity, but are associated with a decrease in the inhibitory phosphorylation of ULK1 (ref. 19) in response to PPARα activation, and an increase in response to FXR activation (Fig. 1b, c and Extended Data Fig. 2a–d). Indeed, GW7647 induces autophagic flux even in non-starved cells, whereas GW4064 suppresses it even in starved cells, or cells treated with the mTOR inhibitor Torin1 (ref. 20) (Extended Data Fig. 1a–e). Activation of FXR by bile acids also suppresses LC3-II induction (Extended Data Fig. 2c).

In livers of chow-fed or fasted wild-type C57BL/6J mice, LC3-II levels were increased in the fasted state (Fig. 2a, b and Extended Data Fig. 2e), and messenger RNA expression of *LC3a* (also known as *Map1lc3a*) and other autophagic genes was also induced (Extended Data Figs 2f and 3a–c). PPARα agonist treatment strongly increased levels of both non-lipidated LC3 (LC3-I) and LC3-II in the fed state in wild-type but not *Ppara*$^{-/-}$ mice[21], and both were further increased in the fasted state (Fig. 2a and Extended Data Fig. 3b). GW7647 also induced *LC3a* mRNA expression in the fed and fasted states, and these responses were lost in *Ppara*$^{-/-}$ mice (Extended Data Fig. 3a).

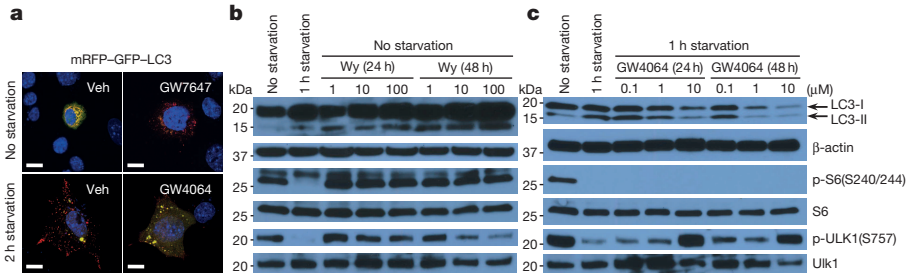

Figure 1 | Activation of PPARα or FXR controls autophagic flux in mouse hepatocytes. **a**, Representative confocal images (out of 30 cells per condition) of AML12 cells transiently expressing mRFP–GFP–LC3 plasmids followed by treatment of vehicle (Veh), GW7647 (100 nM) or GW4064 (10 μM) for 24 h. Cells were starved for 2 h (bottom). DNA was counterstained with 4′,6-diamidino-2-phenylindole (DAPI) (blue). Scale bars, 20 μm. **b**, **c**, Immunoblotting of autophagy (LC3-I/II and p-ULK1(Ser 757)) or mTORC1 activity (p-S6(Ser 240/244)) in AML12 cells treated with indicated doses of Wy-14,643 (Wy) or GW4064 for 24 h or 48 h. GW4064-treated cells were starved for 1 h. kDa, kilodaltons.

[1]Department of Molecular and Cellular Biology, Baylor College of Medicine, Houston, Texas 77030, USA. [2]Division of Endocrinology, Diabetes, and Metabolism and the Institute for Diabetes, Obesity, and Metabolism, Perelman School of Medicine at the University of Pennsylvania, Philadelphia, Pennsylvania 19014, USA. †Present addresses: Laboratory of Experimental Hepatology, Division of Gastroenterology and Hepatology, Department of Internal Medicine, Medical University of Graz, Auenbruggerplatz 15, A-8036 Graz, Austria (M.W.); Stanford University School of Medicine, Palo Alto, California 94305, USA (D.F.).

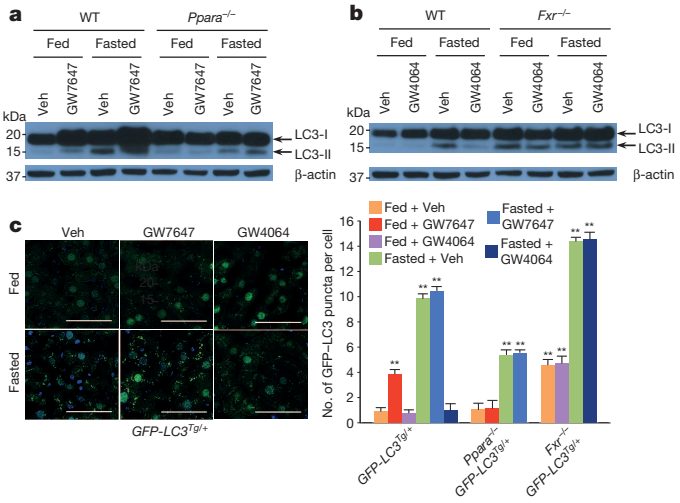

Figure 2 | Activation of PPARα or FXR controls autophagy in liver. **a**, **b**, Fed or fasted *Ppara*$^{-/-}$ (**a**), *Fxr*$^{-/-}$ (**b**) or wild-type (WT) mice treated with GW7647 (**a**), GW4064 (**b**) or vehicle. LC3 immunoblots of mouse liver samples. Lanes are pooled ($n = 5$ per group). **c**, Representative confocal images (out of nine tissues sections per condition) of liver GFP–LC3 puncta (green: autophagosomes), counterstained with DAPI (blue: DNA). Fed or fasted *GFP-LC3*$^{Tg/+}$, bigenic *Ppara*$^{-/-}$ *GFP-LC3*$^{Tg/+}$, or *Fxr*$^{-/-}$ *GFP-LC3*$^{Tg/+}$ mice treated with vehicle, GW7647 or GW4064. Fixed liver samples analysed by confocal microscopy. Scale bars, 50 μm. GFP puncta per cell are quantified in the graph. Data represent mean ± s.e.m. of nine tissue sections ($n = 3$ per group; $^{**}P < 0.01$ versus fed *GFP-LC3*$^{Tg/+}$ mice treated with vehicle; two-tailed *t*-test).

In fed or fasted mice treated with the FXR agonist, induction of LC3-II protein in the fasted state was suppressed in wild-type, but not *Fxr*$^{-/-}$ livers (Fig. 2b and Extended Data Fig. 3d). LC3-II levels were unaffected by GW4064 in fed and fasted *Fxr*$^{-/-}$ mice[22] (Fig. 2b). At the mRNA level, GW4064 completely suppressed the induction of LC3b in the fasted state (Extended Data Fig. 3c). As expected, GW4064 treatment also suppressed CYP7A1, but induced SHP expression in both the fasted and fed states in wild-type, but not *Fxr*$^{-/-}$ mice (Extended Data Figs 2g and 3c).

These results were confirmed using GFP–LC3 transgenic mice (*GFP-LC3*$^{Tg/+}$)[15,16,23] and *GFP-LC3*$^{Tg/+}$ plus *Ppara*$^{-/-}$ or *Fxr*$^{-/-}$ double mutants. Green puncta indicating autophagosome formation were increased in fasted *GFP-LC3*$^{Tg/+}$ mice (Fig. 2c). The PPARα agonist also significantly increased puncta in the fed *GFP-LC3*$^{Tg/+}$ mice, but not in the *Ppara*$^{-/-}$ *GFP-LC3*$^{Tg/+}$ double mutants (Fig. 2c and Extended Data Fig. 3e). In the opposite direction, the FXR agonist strongly suppressed induction of puncta in the fasted *GFP-LC3*$^{Tg/+}$ mice, but not in the fed state, and had no effect in the *Fxr*$^{-/-}$ *GFP-LC3*$^{Tg/+}$ double mutants (Fig. 2c and Extended Data Fig. 3e). The induction of puncta by fasting was significantly lower in the *Ppara*$^{-/-}$ *GFP-LC3*$^{Tg/+}$ double mutants, whereas their number in the fed state was significantly increased in the *Fxr*$^{-/-}$ *GFP-LC3*$^{Tg/+}$ mutants (Fig. 2c and Extended Data Fig. 3e). These partially defective responses in the double mutants demonstrate that PPARα is required for the full induction of autophagy by fasting, and FXR is required for its full suppression by feeding.

In agonist- or vehicle-treated fed and fasted livers, quantification of autophagic vesicles by transmission electron microscopy confirmed an increase in response to GW7647 in the fed state, and a strong decrease in response to GW4064 in the fasted state (Fig. 3a). Moreover, fasted livers of *Ppara*$^{-/-}$ mice show compromised formation of autophagic vesicles but increased numbers and size of lipid droplets. Conversely, livers of fed *Fxr*$^{-/-}$ mice show enhanced formation of autophagic vesicles (Extended Data Fig. 4a, c). Autophagosomes induced by the PPARα agonist frequently contained lipid droplets, suggesting an increase in lipophagy consistent with the role of this receptor in fatty acid oxidation (Extended Data Fig. 4b). This was confirmed in AML12 cells treated with or without oleate to induce lipid droplet formation, and then either starved or not and also treated with vehicle, the PPARα agonist Wy-14,643 or GW4064. Visualization of LC3 (red) revealed colocalization with lipid droplets labelled with the fluorophore dipyrromethene boron difluoride (BODIPY 493/503; green) in the starved cells, as expected, and also in the non-fasted, Wy-14,643-treated cells (Fig. 3b and Extended Data Fig. 3f). In accord with a functional role for the induction of lipophagy, specific knockdown of either Atg5 or Atg7 significantly blunted the increase in fatty acid oxidation in response to Wy-14,643 in basal and oleate-treated AML12 cells, as indicated by ketone body production (Extended Data Fig. 3g). Similarly, both fasting and GW7647 induced serum β-hydroxybutryate levels in control homozygous floxed *Atg7* (*Atg7*$^{F/F}$) mice[24], and both responses were decreased in liver specific *Atg7* knockouts (Extended Data Fig. 3h).

Direct transcriptional effects are the most likely explanation for the effect of both PPARα and FXR on autophagy. Initial results confirmed that total LC3 protein levels are increased and decreased in response to fasting and refeeding, and mRNA expression of *LC3a* and *LC3b* (also known as *Map1lc3b*) and several other autophagic genes is increased in the fasted state and decreased in the refed state (Extended Data Fig. 2e, f). Among a core panel of 63 autophagy-related genes (Supplementary Table 1), 13 were both induced by GW7647 and repressed by GW4064 in wild-type mice, with both responses lost in relevant knockout mice (Fig. 4a and Extended data Fig. 5c), 11 more were responsive only to GW7647, whereas 4 responded only to GW4064 (Extended Data Fig. 5a, b).

To define the basis for PPARα induction of autophagy-related genes, we determined the mouse liver PPARα cistrome with or without GW7647. The most significantly enriched binding motif among identified peaks was the known PPARα–retinoid X receptor (RXR)-binding site (direct repeat 1, or DR1), as expected, and nearly all of the peaks were absent in the *Ppara*$^{-/-}$ cistromes (Extended Data Figs 6a and 7a). PPARα-binding sites on core autophagy machinery gene loci as well as many regulatory and effector genes were confirmed by standard PPARα chromatin

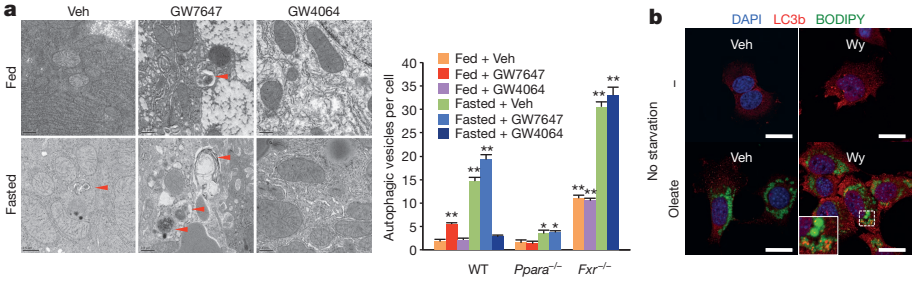

Figure 3 | PPARα and FXR control autophagic vesicle formation in liver. **a**, Representative mouse liver transmission electron micrographs. Fed or fasted wild-type, *Ppara*$^{-/-}$ or *Fxr*$^{-/-}$ mice treated with vehicle, GW7647 or GW4064. Red arrowheads denote autolysosomes. Scale bars, 0.5 μm. Autophagic vesicles (autophagosome/autolysosome) per cell are quantified in the graph. Data represent mean ± s.e.m. for 30 cells per group ($n = 3$ per group; $^{*}P < 0.05$, $^{**}P < 0.01$ versus vehicle-treated fed wild-type mice; two-tailed *t*-test). **b**, Co-localization of BODIPY 493/503 (green) with LC3 (red) in AML12 cells treated with vehicle or 10 μM Wy-14,643 for 24 h, and cultured with or without (−) 125 μM oleate. DNA stained with DAPI (blue). Scale bars, 20 μm.

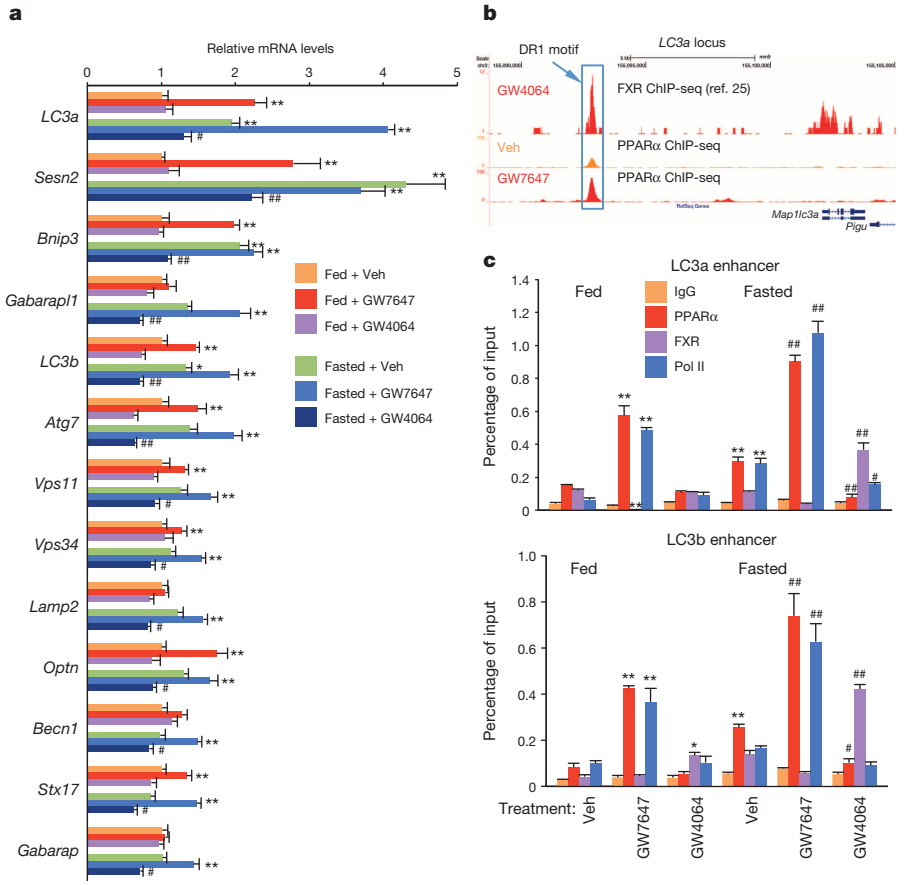

Figure 4 | Transcriptional coordination of hepatic autophagy by nutrient-sensing nuclear receptors *in vivo*. **a**, Hepatic autophagy-related expression of genes controlled by both PPARα and FXR in wild-type mouse liver. Fed or fasted mice treated with vehicle, GW7647 or GW4064 ($n = 5$ per group). *Vps34* is also known as *Pik3c3*. **b**, PPARα and FXR ChIP followed by high-throughput sequencing (ChIP-seq) tracks for LC3a in wild-type mouse liver. Fed wild-type mice treated with vehicle or GW764 ($n = 4$ per group). Boxed peaks contain DR1 motif. **c**, PPARα/FXR binding to LC3a/b DR1 region determined by ChIP-qPCR in wild-type mouse liver ($n = 3$ per group). In **a** and **c**, $*P < 0.05$, $**P < 0.01$ versus vehicle-treated fed wild-type mice; $\#P < 0.05$, $\#\#P < 0.01$ versus vehicle-treated fasted wild-type mice (statistics by two-tailed *t*-test). Data represent mean ± s.e.m.

immunoprecipitation (ChIP) and quantitative PCR (qPCR) analysis (Extended Data Figs 6e and 7). Many of the peaks on these genes (Extended Data Fig. 7a), and an additional panel of key autophagy components including *Pink1*, *Optn*, *Vps11* and *Becn1* (Supplementary Fig. 1), were further enhanced by GW7647 treatment, demonstrating that PPARα agonist treatment not only generates new binding sites, but also further increases PPARα recruitment to specific target genes (Extended Data Fig. 6b).

The PPARα cistrome shows that at least 124 of an extended 230 autophagy-related gene list have at least one receptor binding peak within 20 kilobases (kb) from the transcription start site, while a FXR[25] cistrome shows 61 potential targets (Extended Data Fig. 6d). A hypergeometric test confirmed that both are highly enriched relative to a random gene pool (Extended Data Fig. 6d). Intriguingly, approximately 27% of agonist induced PPARα binding peaks overlapped with 72% of agonist-induced FXR binding peaks (Extended Data Fig. 6c). Consistent with this, peaks for PPARα and FXR directly overlap at 41 out of the 230 extended autophagic target genes, as exemplified by LC3a (Fig. 4b) and LC3b (Extended Data Fig. 8a). This was unexpected, on the basis of their very different direct (PPAR, DR1) and inverted (FXR, inverted repeat 1 (IR1)) repeat consensus binding sites. However, FXR has also been reported to bind DR1 sites in the *Apoc3* (ref. 26) and *Apoa* (ref. 27) promoters, where it acts as a ligand-dependent transcriptional repressor, raising the prospect that it could repress autophagic gene expression via a similar mechanism.

Quantitative assessment confirmed that GW7646 treatment increased PPARα binding to peaks containing a single DR1 site in the LC3a and LC3b enhancers (Fig. 4c) and the *Acox1* promoter (Extended Data Fig. 8a, b), and increased RNA polymerase II recruitment to the genes. Thus, in the fed state, the increased PPARα binding was able to overcome the relatively silent chromatin state and decrease FXR occupancy for the *LC3a* and *Acox1* DR1 sites. In the opposite direction, GW4064 did not have much effect on the already silent chromatin in the fed state, in accord with the functional studies (Figs 2 and 3). In the transcriptionally active fasted state, however, the FXR agonist significantly increased FXR binding, decreased RNA polymerase II recruitment, and also decreased PPARα binding to all three elements (Fig. 4c and Extended Data Fig. 8b). Overall, these results closely match the functional results and indicate that pharmacological activation of each nutrient-sensing nuclear receptor can overcome the chromatin state imposed by the opposite nutrient signal (fed for PPARα and fasted for FXR). They also indicate that PPARα and FXR compete for binding to single sites in some chromatin states.

To test this, we focused on the DR1 motifs in the regulatory region of the *LC3a* and *LC3b* genes. Cell-based reporter assays with promoter constructs including only the DR1 motifs confirmed the opposite responses, with the PPARα agonist further inducing, and the FXR agonist suppressing luciferase expression relative to the increased basal transactivation observed with both PPARα and FXR alone (Extended Data Fig. 8d). In the presence of both receptors, GW4064 suppressed both basal and Wy-14,643-induced expression. Similar results were also observed using a conventional PPAR response element (PPRE) luciferase reporter construct (3×PPRE-luc) (Extended Data Fig. 8c). Mutation of the LC3a or LC3b DR1 elements blocked all responses to PPARα, as expected, but only diminished the responses to FXR (Extended Data Fig. 8d). The basis

for this residual response, which cannot be correlated with direct FXR or FXR–RXR binding *in vitro*, is unclear. The ability of GW4064 to inhibit PPARα-dependent transactivation of the LC3b DR1 motif is dependent on corepressors, because it was blocked by short interfering RNA (siRNA) knockdown of either SMRT or SHP (Extended Data Fig. 8e). Consistent with these functional results, GW7647 treatment increased p300 co-activator recruitment to the DR1 region of LC3a and LC3b enhancers and increased histone H4 acetylation, an active chromatin mark. By contrast, GW4064 treatment increased binding of the corepressors NCoR and SMRT, and increased levels of the repressive histone H3 trimethyl Lys 27 (H3K27me3) mark at the same DR1 regulatory region, particularly in the fasted state (Extended Data Fig. 9). Overall, we conclude that PPARα and FXR directly compete for binding to the same DR1 elements at autophagic, and probably additional promoters, with opposite transcriptional outputs.

This mechanism is distinct from, but complementary to, the inhibition of CRTC2 recruitment described in the accompanying manuscript[28]. Thus, CRTC2 was not significantly recruited to the LC3a DR1 enhancer, as expected, but we confirmed the ability of GW4064 treatment to decrease CRTC2 occupancy to its proximal promoter site in the fasted state (Extended Data Fig. 10a).

These results define new mechanisms for regulation of autophagy by nutrient-sensing nuclear receptors (Extended Data Fig. 10b). Pharmacological activation of either PPARα or FXR robustly affects hepatic autophagy. GW7467 activates it even in the fed state, which is associated with an increase in lipophagy. GW4064 potently suppresses the process in the fasted state. The significantly blunted autophagic responses of PPARα and FXR knockouts to fasting or feeding, respectively, strongly confirm the physiological relevance of the pharmacologically defined responses.

Both nuclear receptors directly induce or repress extensive panels of autophagy-related genes in accord with the overall responses. However, the effect of the synthetic agonists seems greater than the magnitude of the transcriptional responses, suggesting a role for less direct effects. We did not observe effects on mTOR, the dominant upstream regulator of autophagy. However, there were alterations in the inhibitory phosphorylation of ULK1(Ser 757) that would be consistent with such effects. In addition, induction of the transcriptional repressor SHP is a well-described mechanism for FXR-dependent suppression of genes of bile acid biosynthesis[29,30]. However, preliminary results indicate that the suppressive effects of GW4064 are maintained in $Shp^{-/-}$ (also known as $Nr0b2^{-/-}$) mice (data not shown).

These results reveal intersecting and complementary genomic circuits in which PPARα and FXR induce and suppress hepatic autophagy, respectively (Extended Data Fig. 10b). They further integrate autophagy, which is often associated with more extreme nutrient stresses, with more physiological nutrient responses. They also establish PPARα and FXR as potential targets for therapeutic modulation autophagy, which may be useful for liver or other metabolic tissues and could affect the pathogenesis of a wide range of human diseases.

Online Content Methods, along with any additional Extended Data display items and Source Data, are available in the online version of the paper; references unique to these sections appear only in the online paper.

Received 1 October 2013; accepted 13 October 2014.
Published online 12 November 2014.

1. Mizushima, N., Levine, B., Cuervo, A. M. & Klionsky, D. J. Autophagy fights disease through cellular self-digestion. *Nature* **451,** 1069–1075 (2008).
2. Levine, B. & Kroemer, G. Autophagy in the pathogenesis of disease. *Cell* **132,** 27–42 (2008).
3. Rabinowitz, J. D. & White, E. Autophagy and metabolism. *Science* **330,** 1344–1348 (2010).
4. Evans, R. M., Barish, G. D. & Wang, Y. X. PPARs and the complex journey to obesity. *Nature Med.* **10,** 355–361 (2004).
5. Chawla, A., Saez, E. & Evans, R. M. Don't know much bile-ology. *Cell* **103,** 1–4 (2000).
6. Nordlie, R. C., Foster, J. D. & Lange, A. J. Regulation of glucose production by the liver. *Annu. Rev. Nutr.* **19,** 379–406 (1999).
7. Laplante, M. & Sabatini, D. M. mTOR signaling in growth control and disease. *Cell* **149,** 274–293 (2012).
8. Inoki, K., Kim, J. & Guan, K. L. AMPK and mTOR in cellular energy homeostasis and drug targets. *Annu. Rev. Pharmacol. Toxicol.* **52,** 381–400 (2012).
9. Hardie, D. G., Ross, F. A. & Hawley, S. A. AMPK: a nutrient and energy sensor that maintains energy homeostasis. *Nature Rev. Mol. Cell Biol.* **13,** 251–262 (2012).
10. Settembre, C. & Ballabio, A. Lysosome: regulator of lipid degradation pathways. *Trends Cell Biol.* http://dx.doi.org/10.1016/j.tcb.2014.06.006 (21 July 2014).
11. Göttlicher, M., Widmark, E., Li, Q. & Gustafsson, J. A. Fatty acids activate a chimera of the clofibric acid-activated receptor and the glucocorticoid receptor. *Proc. Natl Acad. Sci. USA* **89,** 4653–4657 (1992).
12. Keller, H. *et al.* Fatty acids and retinoids control lipid metabolism through activation of peroxisome proliferator-activated receptor-retinoid X receptor heterodimers. *Proc. Natl Acad. Sci. USA* **90,** 2160–2164 (1993).
13. Ma, K., Saha, P. K., Chan, L. & Moore, D. D. Farnesoid X receptor is essential for normal glucose homeostasis. *J. Clin. Invest.* **116,** 1102–1109 (2006).
14. Kimura, S., Noda, T. & Yoshimori, T. Dissection of the autophagosome maturation process by a novel reporter protein, tandem fluorescent-tagged LC3. *Autophagy* **3,** 452–460 (2007).
15. Mizushima, N., Yoshimori, T. & Levine, B. Methods in mammalian autophagy research. *Cell* **140,** 313–326 (2010).
16. Klionsky, D. J. *et al.* Guidelines for the use and interpretation of assays for monitoring autophagy. *Autophagy* **8,** 445–544 (2012).
17. Maloney, P. R. *et al.* Identification of a chemical tool for the orphan nuclear receptor FXR. *J. Med. Chem.* **43,** 2971–2974 (2000).
18. Brown, P. J. *et al.* Identification of a subtype selective human PPARα agonist through parallel-array synthesis. *Bioorg. Med. Chem. Lett.* **11,** 1225–1227 (2001).
19. Kim, J., Kundu, M., Viollet, B. & Guan, K. L. AMPK and mTOR regulate autophagy through direct phosphorylation of Ulk1. *Nature Cell Biol.* **13,** 132–141 (2011).
20. Thoreen, C. C. *et al.* An ATP-competitive mammalian target of rapamycin inhibitor reveals rapamycin-resistant functions of mTORC1. *J. Biol. Chem.* **284,** 8023–8032 (2009).
21. Lee, S. S. *et al.* Targeted disruption of the α isoform of the peroxisome proliferator-activated receptor gene in mice results in abolishment of the pleiotropic effects of peroxisome proliferators. *Mol. Cell. Biol.* **15,** 3012–3022 (1995).
22. Sinal, C. J. *et al.* Targeted disruption of the nuclear receptor FXR/BAR impairs bile acid and lipid homeostasis. *Cell* **102,** 731–744 (2000).
23. Mizushima, N., Yamamoto, A., Matsui, M., Yoshimori, T. & Ohsumi, Y. In vivo analysis of autophagy in response to nutrient starvation using transgenic mice expressing a fluorescent autophagosome marker. *Mol. Biol. Cell* **15,** 1101–1111 (2004).
24. Komatsu, M. *et al.* Impairment of starvation-induced and constitutive autophagy in Atg7-deficient mice. *J. Cell Biol.* **169,** 425–434 (2005).
25. Thomas, A. M. *et al.* Genome-wide tissue-specific farnesoid X receptor binding in mouse liver and intestine. *Hepatology* **51,** 1410–1419 (2010).
26. Claudel, T. *et al.* Farnesoid X receptor agonists suppress hepatic apolipoprotein CIII expression. *Gastroenterology* **125,** 544–555 (2003).
27. Chennamsetty, I. *et al.* Farnesoid X receptor represses hepatic human *APOA* gene expression. *J. Clin. Invest.* **121,** 3724–3734 (2011).
28. Seok, S. *et al.* Transcriptional regulation of autophagy by an FXR–CREB axis. *Nature* http://dx.doi.org/10.1038/nature13949 (this issue).
29. Kerr, T. A. *et al.* Loss of nuclear receptor SHP impairs but does not eliminate negative feedback regulation of bile acid synthesis. *Dev. Cell* **2,** 713–720 (2002).
30. Wang, L. *et al.* Redundant pathways for negative feedback regulation of bile acid production. *Dev. Cell* **2,** 721–731 (2002).

Supplementary Information is available in the online version of the paper.

Acknowledgements We thank N. Mizushima for the *GFP-LC3*$^{Tg/+}$ mice; T. Yoshimori for the mRFP–GFP–LC3 plasmid; M. Komatsu for the *Atg7*$^{F/F}$ mice; D. Townley and M. Mancini for transmission electron microscopy and confocal microscopy; the members of the Moore laboratory for comments and additional support. Core facilities supported by grants U54 HD-07495-39, P30 DX56338-05A2, P39 CA125123-04 and S10RR027783-01A1. Next-generation sequencing was performed by the Functional Genomics Core of the Penn Diabetes Research Center (DK19525). This work was supported by funding from the Alkek Foundation and the Robert R. P. Doherty Jr-Welch Chair in Science to D.D.M., and R01 DK49780 and DK43806 to M.A.L.

Author Contributions J.M.L. conceived the project, designed and performed most experiments, interpreted results, and co-wrote the manuscript. M.W. performed animal experiments and participated in discussion of the results. R.X. analysed PPARα and FXR ChIP-seq data, and designed primers for PPARα ChIP-qPCR. K.H.K. performed ChIP assays and molecular cloning. D.F. performed PPARα ChIP-seq. M.A.L. supervised experimental designs. D.D.M. conceived the project, supervised experimental designs, interpreted results, and co-wrote the manuscript.

Author Information PPARα ChIP-seq data sets have been deposited in the NCBI Gene Expression Omnibus with the accession number GSE61817. Reprints and permissions information is available at www.nature.com/reprints. The authors declare no competing financial interests. Readers are welcome to comment on the online version of the paper. Correspondence and requests for materials should be addressed to D.D.M. (moore@bcm.edu).

METHODS

Materials. C57BL/6J and *Ppara*$^{-/-}$ mice were from the Jackson Laboratory; *Fxr*$^{-/-}$ and *GFP-LC3* transgenic mice were previously described[23]. Antibodies to LC3 (NB600-1384) were from Novus Biologicals; rabbit antibodies to phosphorylated Ser 240/244 S6 (5364), S6 (2217), phosphorylated Thr 37/46-4E-BP1 (2855), 4E-BP1 (9452), anti-mouse IgG–horseradish peroxidise (HRP) (7076) and β-actin (5125) were from Cell Signaling Technology; antibodies to normal rabbit IgG (sc-2027), PPARα (sc-9000x), FXR (sc-13063x), Pol II (sc-899x), p300 (sc-585x), CRTC2/TORC2 (sc-6714x) and anti-rabbit IgG-HRP (sc-2370) were from Santa Cruz Biotechnology; antibody to histone H3K27me3 (39155) was from ACTIVE MOTIF. GW7647 and Wy-14,643 were from Cayman chemicals; GW4064 was from Tocris bioscience; bafilomycin A_1 was from Enzo Life Science; AML12 cells were from ATCC (CRL-2254). GFP antibody (11814460001), PhosSTOP (04906837001) and complete protease cocktail (11836170001) were from Roche; insulin-transferrin-selenium (ITS) (41400-045), lipofectamine 2000 (11668019), BODIPY 493/503 (D-3922), Alexa Fluor 594 goat anti-rabbit IgG (A11037), Stealth siRNAs-NCoR (NcoR1, MSS208758), SMRT (NcoR2, MSS20912), SHP (NR0b2, MSS239500) and HIGH_GC were from Invitrogen. The mRFP–GFP–LC3(ptfLC3) plasmid was a gift from T. Yoshimori (Addgene plasmid 21074). Anti-rabbit p62/SQSTM1 (P0067), anti-rabbit LC3B (L7543), oleic-acid-albumin (O3008-5ML) and dexamethasone (D4902-25MG) were from Sigma. Protein A Sepharose CL-48 (17-0780-01) was from GE Healthcare; VECTASHIELD (H-1200) was from Vector Laboratories; SacI-HF (R3156S) and BglII (R0144S) were from New England Biolabs. Pierce BCA Protein Assay Kit (23227) was from Thermo Scientific; SMRT antibody (ab24551) and β-hydroxybutyrate assay kit (ab83390) were from abcam. Anti-acetyl-histone H4 antibody (06-866) was from EMD Millipore. Polyclonal rabbit antibody against NCoR was as described[33]. Other reagent information not shown here is described in the relevant methods and references.

Animal studies. All animal studies and procedures were approved by the institutional Animal Care and Use Committee of the Baylor College of Medicine. Male *GFP-LC3*$^{Tg/+}$ mice were bred with either female *Ppara*$^{-/-}$ or *Fxr*$^{-/-}$ mice to generate bigenic *Ppara*$^{-/-}$ *GFP-LC3*$^{Tg/+}$ or *Fxr*$^{-/-}$ *GFP-LC3*$^{Tg/+}$ mice. *Ppara*$^{-/-}$ and *Fxr*$^{-/-}$ mice were pure C57BL/6 background. C57BL/6J mice were wild-type controls. Eight-to-ten-week-old male wild-type C57BL/6J, *Ppara*$^{-/-}$, *Fxr*$^{-/-}$, *GFP-LC3*$^{Tg/+}$, *Ppara*$^{-/-}$ *GFP-LC3*$^{Tg/+}$ or *Fxr*$^{-/-}$ *GFP-LC3*$^{Tg/+}$ mice were orally gavaged with vehicle (dimethylsulphoxide (DMSO) in 4:1 of PEG-400 and Tween 80), GW7647 (5 mg kg^{-1} body weight) or GW4064 (100 mg kg^{-1} body weight) twice a day (first injection: 00:00, second injection: 12:00). Mice were fed *ad libitum* or fasted for 24 h from 18:00 (day 1) to 18:00 (day 2) and then scarified to collect blood and livers. Collected liver tissues were immediately frozen in liquid nitrogen for molecular studies. The refed condition was 24 h fasted mice followed by feeding those mice with normal chow diets for another 24 h. To avoid circadian issues, all mice were scarified at 17:00–18:00. *GFP-LC3*$^{Tg/+}$ mice were a gift from N. Mizushima.

Primary hepatocyte culture. Eight-to-ten-week-old male *GFP-LC3*$^{Tg/+}$ mice were anesthetized with Avertin (Sigma Aldrich, T48402, 240 mg kg^{-1} body weight) by intraperitoneal (i.p.) injection. The liver perfusions were done by injecting butterfly needle into the portal vein and providing the following solutions sequentially: 50 ml EBSS (ATLANTA biologicals, B31350) supplemented with 10 mM HEPES (Invitrogen, 24020-117) and 0.5 mM EGTA and then 50 ml of HBSS supplemented with 100 U ml^{-1} of collagenase IV (Invitrogen, 17101-015), and 0.05 mg ml^{-1} of trypsin inhibitor (Invitrogen, 17075-029). The perfused liver was carefully taken out, put onto a Petri dish with 25 ml of hepatocyte wash media added (Invitrogen, 17704-024), and massaged with two cell scrapers until the liver came apart with only connective tissue left behind. Dissociated cells were passed through a mesh funnel into a 50 ml falcon tube. After centrifugation at 600 r.p.m. for 2 min, the cell pellet was resuspended in hepatocyte wash media consisting of carefully overlaid Percoll solution (final 40%) pre-mixed with 150 mM NaCl. After centrifugation at 600 r.p.m. for 10 min, the collected cell pellet was washed twice with hepatocyte wash media, and then suspended in Williams' E medium (Invitrogen, 12551-032) supplemented with 10% FBS, 1% penicillin/streptomycin, ITS and glutaMAX (Invitrogen, 35050-061). All drug treatments or starvation experiments were performed 4–6 h after the initial plating on the culture dishes.

Cell culture and transfection. AML12 cells were maintained in the following media: (normal) DMEM/F12 high glucose (Invitrogen, 11330-057) supplemented with 10% FBS, 1% ITS, 1% penicillin/streptomycin antibiotics and 40 ng ml^{-1} dexamethasone; (starvation) HBSS media with Ca^{2+} and Mg^{2+} supplemented with 10 mM HEPES (Invitrogen, 15630). mRFP–GFP–LC3 plasmids were transfected into AML12 cells grown on Lab-tek II Chamber Slide (Nunc, 154461) with Lipofectamine 2000 according to the manufacturer's protocol for 24 h followed by drug treatments for 24 h. Transfected cells were starved for 2 h, and then washed three times with cold PBS, fixed with 3% paraformaldehyde (PFA) in PBS for 10 min at room temperature, and washed three times with PBS. Cells were counterstained with mounting solution containing DAPI. All drugs were dissolved in DMSO. Vehicle: complete media containing 0.1% DMSO. Starvation: HBSS media with 10 mM HEPES. Autophagic fluxes were quantified as follows: autolysosomes = RFP-positive vesicles – GFP-positive vesicles. Numbers of autolysosomes induced by 2 h starvation plus vehicle were set as 100%.

BODIPY and immunofluorescence assay in cells. AML12 cells were plated on two-chamber Lab-tek II dishes at 30–50% confluent cells per chamber. The next day, cells were treated with vehicle (0.1% DMSO), 10 μM Wy-14,643 or 1 μM GW4064 in complete medium with or without 125 μM oleate for 24 h. Vehicle or GW4064-treated cells were starved for 2 h in HBSS medium before fixation of cells. Cells were washed twice with PBS followed by fixation with 3% PFA for 20 min at room temperature. After fixation, cells were washed four times with PBS followed by incubation with blocking buffer (1.5 g glycine, 3 g BSA and 2 ml 0.5% (w/v) saponin in 100 ml PBS) for 45 min. Cells were incubated with rabbit anti-LC3b antibody (1:400 dilution in antibody diluent: 100 mg BSA, 2 ml 0.5% saponin in 100 ml PBS) overnight at 4 °C. Cells were washed four times (10 min each) with PBS followed by incubation with the secondary antibody (Alexa Fluor 594 goat anti-rabbit IgG, 1:200 dilution in antibody diluent) and BODIPY 493/503 (1 μg ml^{-1} concentration) for 1 h at room temperature. After that, cells were washed four times with PBS followed by DAPI staining with mounting solution. Cell images were obtained using a confocal microscope (NIKON A1Rsi dual scanner). Orange and yellow dots were defined as a lipophagic vacuole, which was quantified in at least in 30 cells per condition using ImageJ software.

RNA purification and qPCR analysis. Total RNA was isolated from snap-frozen liver tissues using Trizol Reagent (Invitrogen, 15596-026) and prepared for the complementary DNA using QuantiTect reverse transcription kit (Qiagen, 205311). Hepatic gene expression was determined by qPCR using FastStart SYBR Green master (ROX) (Roche, 04673484001). mRNA levels were normalized by the *36B4* (also known as *Rplp0*) gene. qPCR primer information for autophagy-related genes is listed in Supplementary Table 1, and all other primers were purchased from Qiagen.

Immunoblot analysis. Cells cultured in 10-cm dishes were solubilized in 150 μl of RIPA buffer (25 mM Tris-HCl, pH 7.6, 150 mM NaCl, 1% NP-40, 1% sodium deoxycholate, 0.1% SDS and 1 mM EDTA) supplemented with protease and phosphatase inhibitors. Liver tissues (50 mg) were homogenized in 1 ml RIPA buffer supplemented with protease and phosphatase inhibitors, followed by brief sonication. Protein concentration was determined using Pierce BCA Protein Assay Kit. Total proteins (25–50 μg) were loaded on either 12% or 4–20% Mini-PROTEAN TGX Precast Gel (Bio-rad, 456-1043 or 456-1093), transferred onto Immuno-Blot PVDF (polyvinylidene difluoride) membrane (Bio-rad, 162-0177) and analysed by immunoblot analysis using the ECL solution (Thermo Scientific, 34086, or Millipore, WBKLS0500).

Histology and immunofluorescence. Liver tissues were collected and fixed in 4% PFA in PBS overnight at 4 °C. The tissues were treated with 15% sucrose in PBS at 4 °C for at least 4 h and then with 30% sucrose in PBS at 4 °C for overnight. Tissue samples were embedded in Tissue-Tek OCT (Sakura Finetek, 4583) and stored at −70 °C. The samples were sectioned at 5–7 μm thickness, air-dried for 30 min, and stored at −20 °C until use (Comparative Pathology Laboratory at Baylor College of Medicine). Images were taken on a confocal microscope (NIKON A1Rsi dual scanner). GFP–LC3 puncta were quantified in three independent visual fields from at least three independent mice using ImageJ software.

ChIP assays. ChIP from mouse livers was performed as described previously[34]. For PPARα ChIP-seq and ChIP-qPCR (Extended Data Fig. 7), livers were collected from fed wild-type or *Ppara*$^{-/-}$ mice treated with vehicle or GW7647 (5 mg kg^{-1}, twice a day, $n = 4$ per group) after euthanasia. For PPARα, FXR, Pol II, p300, CRTC2 (TORC2), NCoR, SMRT, acetyl H4 and H3K27me3 ChIPs (Fig. 4c and Extended Data Figs 9 and 10a), fed or fasted wild-type mice were treated with vehicle, GW7647 (5 mg kg^{-1}) or GW4064 (100 mg kg^{-1}) twice a day ($n = 3$ per group). Liver tissues (100 mg) were quickly minced using mortar and pestle with liquid nitrogen and cross-linked in 10 ml 1% formaldehyde/PBS for 15 min at room temperature, followed by quenching with 1/20 volume of 2.5 M glycine solution for 5 min. Minced liver tissues were washes twice with cold PBS (150 g, 5 min, 4 °C). Nuclear extracts were prepared by Dounce homogenization (30 strokes on ice, tight fitting pestle-type B) in cell lysis buffer (5 mM PIPES, 85 mM KCl, 0.5% Igepal and complete protease inhibitor tablet from Roche, pH 8.0). Chromatin fragmentation was performed by sonication in 300 μl ChIP SDS lysis buffer (50 mM HEPES, 1% SDS, 10 mM EDTA, pH 7.5), using the Bioruptor (Diagenode, 4 × 5 min, 30 s on/30 s off). Proteins of interest were immunoprecipitated in ChIP dilution buffer (50 mM HEPES, 155 mM NaCl, 1.1% Triton X-100, 0.11% sodium deoxycholate, 1 mM phenylmethylsulphonyl fluoride (PMSF) and complete protease inhibitors tablet, pH 7.5) using 5 μl of each antibody. Cross-linking was reversed overnight at 65 °C, and DNA was isolated using phenol/chloroform/isoamyl alcohol. Precipitated DNA was analysed by qPCR. Primer sequences used for ChIP-qPCR analysis are listed in Supplementary Table 2.

PPARα ChIP-seq. For ChIP, frozen liver tissues were ground in liquid nitrogen and cross-linked in 1% formaldehyde for 20 min, followed by quenching with 1/20 volume of 2.5 M glycine solution, and two washes with PBS. Cell lysis and chromatin fragmentation were performed by sonication in ChIP dilution buffer (50 mM HEPES, 155 mM NaCl, 1.1% Triton X-100, 1% SDS, 0.11% sodium deoxycholate, 1 mM EDTA, and complete protease inhibitors tablet, pH 7.5). PPARα proteins were immunoprecipitated using PPARα antibody, cross-linking was reversed overnight at 65 °C, and DNA was isolated using phenol/chloroform/isoamyl alcohol. Precipitated DNA was analysed by qPCR. ChIP was performed independently on liver samples from fed wild-type or *Ppara*$^{-/-}$ mice treated with vehicle or GW7647 (5 mg kg^{-1}, twice a day), and the precipitated DNA or input DNA samples were pooled. Ten nanograms of the pooled DNA was then amplified according to ChIP Sequencing Sample Preparation Guide provided by Illumina, using adaptor oligonucleotides and primers from Illumina, enzymes from New England Biolabs and the PCR Purification Kit and MinElute Kit from Qiagen. Deep sequencing was performed by the Functional Genomics Core (J. Schug and K. Kaestner) of the Penn Diabetes Endocrinology Research Center using the Illumina Genome Analyzer IIx, and sequences were obtained using the Solexa Analysis Pipeline.

ChIP-seq data analysis. Solexa sequencing reads were mapped to reference genome mm9 using Bowtie[35]. Peak calling was performed with MACS14 using default settings[36]. Peak heights were normalized to the total number of uniquely mapped reads and displayed in UCSC genome browser[37] as the number of tags per 10 million tags. *De novo* motif analysis was performed with MEME[31] using 200-bp regions centred at the summit of each peak. To analyse the enrichment of autophagy-related genes near PPARα-binding sites, all genes containing a PPARα-binding site (with or without the PPARα motif DR1) within 20 kb from the transcription start site were compared with a list of autophagy-related genes[32,38–44] (Supplementary Table 1). *P* values were calculated with hypergeometric test.

Transmission electron microscopy. Anaesthetized mice were perfused with PBS for 3 min, followed immediately by perfusion with 2% PFA plus 2.5% glutaraldehyde in 0.1 M Millonig's phosphate buffer, pH 7.4. Liver tissue was quickly removed and minced in a large drop of cold fixative, then transferred to vials of cold fix and fixed overnight in 4 °C. After washing three times in 0.1 M Millonig's phosphate buffer, the tissue was post-fixed at room temperature in 0.1 M Millonig's phosphate buffer containing 1% osmium tetroxide for 1 h. Post-fixation was followed by three rinses, 5 min each, of 0.1 M Millonig's phosphate buffer, after which all tissues were dehydrated through a gradient series of ethanol, beginning with two 10 min changes of 50% ethanol and ending with three 20 min changes of 100% ethanol from a freshly opened bottle. Liver tissue was en bloc stained with saturated uranyl acetate in 50% ethanol for 1 h during the 50% ethanol dehydration stage. After complete dehydration, the tissue was infiltrated over a period of 2 days with progressively concentrated mixtures of plastic resin and 100% ethanol. Infiltration continued until the tissue reached pure resin. The tissue was then given three changes of pure, freshly made Spurr's plastic resin[45] for 3 h each, after which the liver tissue was embedded in 00 BEEM capsules[46] and placed in a 68 °C oven overnight. Thin sections of approximately 70 nm were obtained using an RMC MT6000-XL ultramicrotome (RMC) and a Diatome Ultra45 diamond knife (DiATOME), and collected on 150 hex-mesh copper grids. The sections were counterstained with Reynold's lead citrate[47] for 4 min. Dry samples were examined on a Hitachi H7500 transmission electron microscope and images were captured using a Gatan US1000 digital camera with Digital Micrograph (Gatan, v1.82.366) software.

Molecular cloning and cell-based luciferase reporter assay. The oligonucleotides encompassing three copies of DR1 motifs found in mouse LC3a or LC3b enhancer region were annealed and treated with Klenow. Purified DNAs were cloned into pTK-luc plasmid by a serial digesting with SacI and BglII. Successful cloning was confirmed by DNA sequencing analysis. Oligonucleotide sequences used for luciferase reporter assays are listed in Supplementary Table 3. For the luciferase assay, AML12 cells were cultured in 24-well plates. Transient transfections were performed using Lipofectamine 2000. Cell were transfected with 200 ng of reporter constructs, 100 ng of cytomegalovirus-promoter (CMX)-mouse PPARα, or CMX-human FXR, and 50 ng of CMX-β-galactosidase. pCDNA3.1 was added to prepare the total DNA to 500 ng per well. After 4 h transfection, cells were treated with or vehicle (0.1% DMSO), 10 μM Wy-14,643 or 1 μM GW4064 in media containing charcoal-stripped serum for 20 h before performing luciferase and β-galactosidase assay. Luciferase activity was normalized with β-galactosidase activity. Normalized values from vehicle-treated cells transfected with empty CMX plasmid were set as fold 1.

Measurement of β-hydroxybutyrate. AML12 cells were transfected with siControl (ON-TARGETplus Control pool, D-001810-10-20), siAtg5 (ON-TARGETplus SMARTpool siRNA Atg5, L-064838-00-0010), or siAtg7 (ON-TARGETplus SMARTpool siRNA Atg7, L-049953-00-0010) according to manufacturer's instructions. siRNAs were purchased from Thermo Scientific Dharmacon. Twenty-four hours after transfection using Lipofectamine 2000, cells were treated with vehicle (0.1% DMSO) or Wy-14,643 (10 μM) in media containing charcoalstripped serum and 250 μM oleate for 48 h. Released β-hydroxybutyrate in the medium was measured using a β-hydroxybutyrate assay kit. Female *Atg7*$^{F/F}$ mice[24] were bred with male *Alb-Cre*/+ mice to generate control littermates (*Atg7*$^{F/F}$) and hepatocyte-specific *Atg7*-null (Alb-Cre/+ *Atg7*$^{F/F}$) mice. Eight-week-old male *Atg7*$^{F/F}$ and *Alb-Cre*/+ *Atg7*$^{F/F}$ mice were orally gavaged with either vehicle (DMSO in 4:1 of PEG-400 and Tween 80) or GW7647 (5 mg kg^{-1} body weight) twice a day (first injection: 00:00, second injection: 12:00). Mice were fed *ad libitum* or fasted for 24 h from 18:00 (day 1) to 18:00 (day 2) and then scarified to collect blood and livers. Serum β-hydroxybutyrate concentrations were normalized with mouse liver weights.

Statistical analysis. Sample size for experiments was determined empirically based on preliminary experiments to ensure appropriate statistical power. Age, sex and weight-matched mice were randomly assigned for the treatments. No animals were excluded from statistical analysis, and the investigators were not blinded in the studies. Values are expressed as mean ± s.e.m., and error bars for all results were derived from biological replicates rather than technical replicates. Significant differences between two groups were evaluated using a two-tailed, unpaired *t*-test, which was found to be appropriate as groups displayed a normal distribution and comparable variance. $P < 0.05$ was considered statistically significant.

31. Bailey, T. L. *et al.* MEME SUITE: tools for motif discovery and searching. *Nucleic Acids Res.* **37,** W202–W208 (2009).
32. Mizushima, N., Yoshimori, T. & Ohsumi, Y. The role of Atg proteins in autophagosome formation. *Annu. Rev. Cell Dev. Biol.* **27,** 107–132 (2011).
33. Sun, Z. *et al.* Deacetylase-independent function of HDAC3 in transcription and metabolism requires nuclear receptor corepressor. *Mol. Cell* **52,** 769–782 (2013).
34. Feng, D. *et al.* A circadian rhythm orchestrated by histone deacetylase 3 controls hepatic lipid metabolism. *Science* **331,** 1315–1319 (2011).
35. Langmead, B., Trapnell, C., Pop, M. & Salzberg, S. L. Ultrafast and memory-efficient alignment of short DNA sequences to the human genome. *Genome Biol.* **10,** R25 (2009).
36. Zhang, Y. *et al.* Model-based analysis of ChIP-Seq (MACS). *Genome Biol.* **9,** R137 (2008).
37. Kent, W. J. *et al.* The human genome browser at UCSC. *Genome Res.* **12,** 996–1006 (2002).
38. Kundu, M. & Thompson, C. B. Autophagy: basic principles and relevance to disease. *Annu. Rev. Pathol.* **3,** 427–455 (2008).
39. Jin, M., Liu, X. & Klionsky, D. J. SnapShot: Selective autophagy. *Cell* **152,** 368–368 (2013).
40. Settembre, C. *et al.* TFEB links autophagy to lysosomal biogenesis. *Science* **332,** 1429–1433 (2011).
41. Warr, M. R. *et al.* FOXO3A directs a protective autophagy program in haematopoietic stem cells. *Nature* **494,** 323–327 (2013).
42. Shoji-Kawata, S. *et al.* Identification of a candidate therapeutic autophagy-inducing peptide. *Nature* **494,** 201–206 (2013).
43. Itakura, E., Kishi-Itakura, C. & Mizushima, N. The hairpin-type tail-anchored SNARE syntaxin 17 targets to autophagosomes for fusion with endosomes/lysosomes. *Cell* **151,** 1256–1269 (2012).
44. McKnight, N. C. *et al.* Genome-wide siRNA screen reveals amino acid starvation-induced autophagy requires SCOC and WAC. *EMBO J.* **31,** 1931–1946 (2012).
45. Spurr, A. R. A low-viscosity epoxy resin embedding medium for electron microscopy. *J. Ultrastruct. Res.* **26,** 31–42 (1969).
46. Glauert, A. M. *Practical Methods in Electron Microscopy* 143–144 (North-Holland American Elsevier, 1975).
47. Reynolds, E. S. The use of lead citrate at high pH as an electron-opaque stain in electron microscopy. *J. Cell Biol.* **17,** 208–212 (1963).

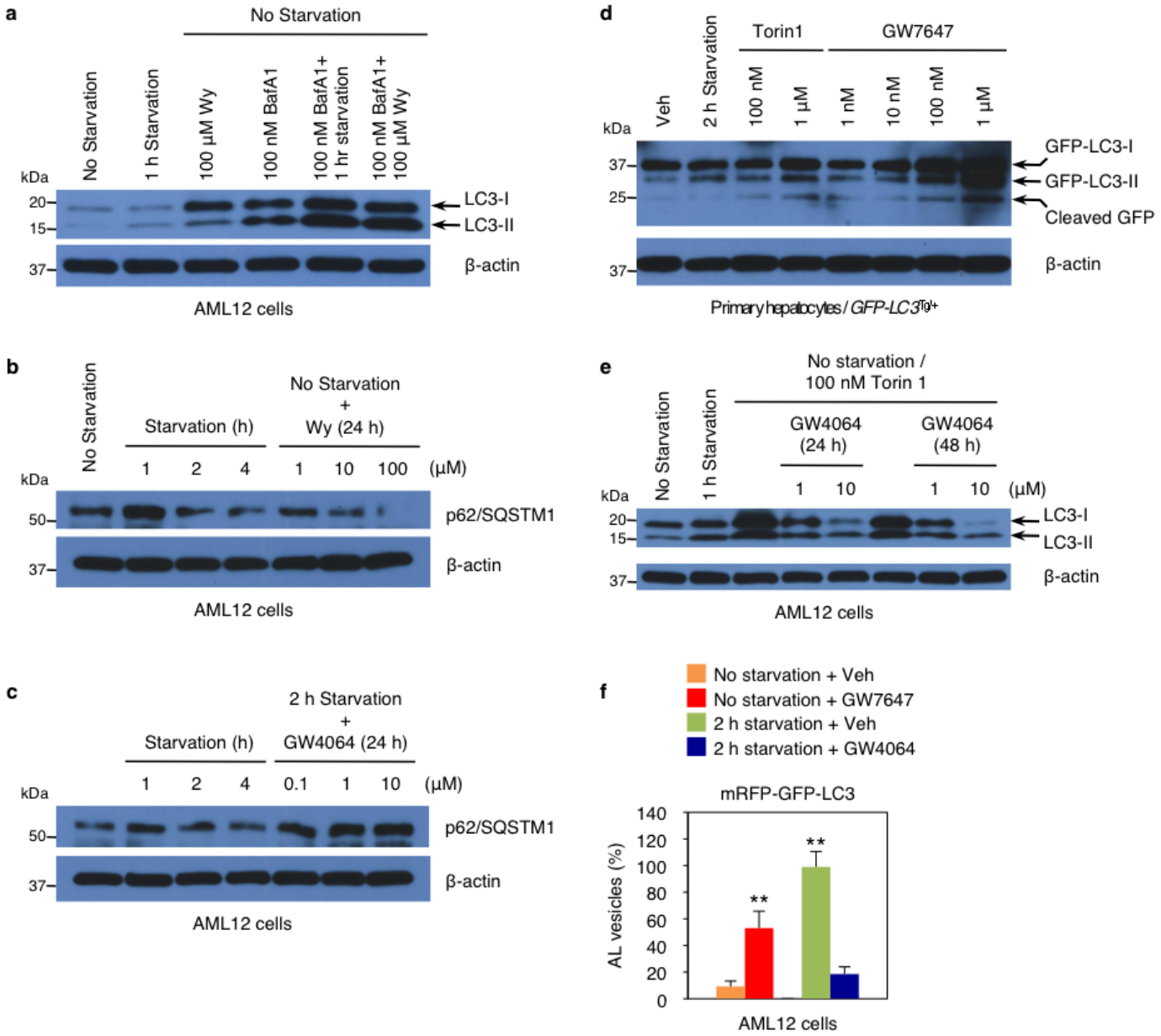

Extended Data Figure 1 | PPARα or FXR agonist affects autophagic flux in mouse hepatocytes. **a**, Autophagic flux was assessed by LC3 immunoblot analysis in AML12 cells treated with indicated dose of Wy-14,643, or co-treated with both Wy-14,643 and bafilomycin A_1 (BafA1). **b**, **c**, Biochemical determination of autophagy (p62/SQSTM1 immunoblot) in AML12 cells treated with indicated doses of Wy-14,643 or GW4064 for 24 h. GW4064-treated cells were starved for 2 h. **d**, Primary hepatocytes from *GFP-LC3*$^{Tg/+}$ mice were treated with indicated doses of Torin1 or GW7647. GFP–LC3 cleavage was assessed by GFP immunoblot analysis. **e**, LC3 immunoblot in AML12 cells treated with indicated doses of GW4064 or co-treated with GW4064 and Torin1. All drug treatments were done in complete media for 24 h unless otherwise indicated. β-actin is a loading control. **f**, Quantification of autophagic flux shown in Fig. 1a. Numbers of autolysosomes (ALs) induced by 2 h starvation plus vehicle were set as 100%. Numbers of autolysosomes = RFP-positive vesicles – GFP-positive vesicles. Thirty cells were counted per condition (**$P < 0.01$ versus no starvation plus vehicle; two-tailed *t*-test). Data represent mean ± s.e.m.

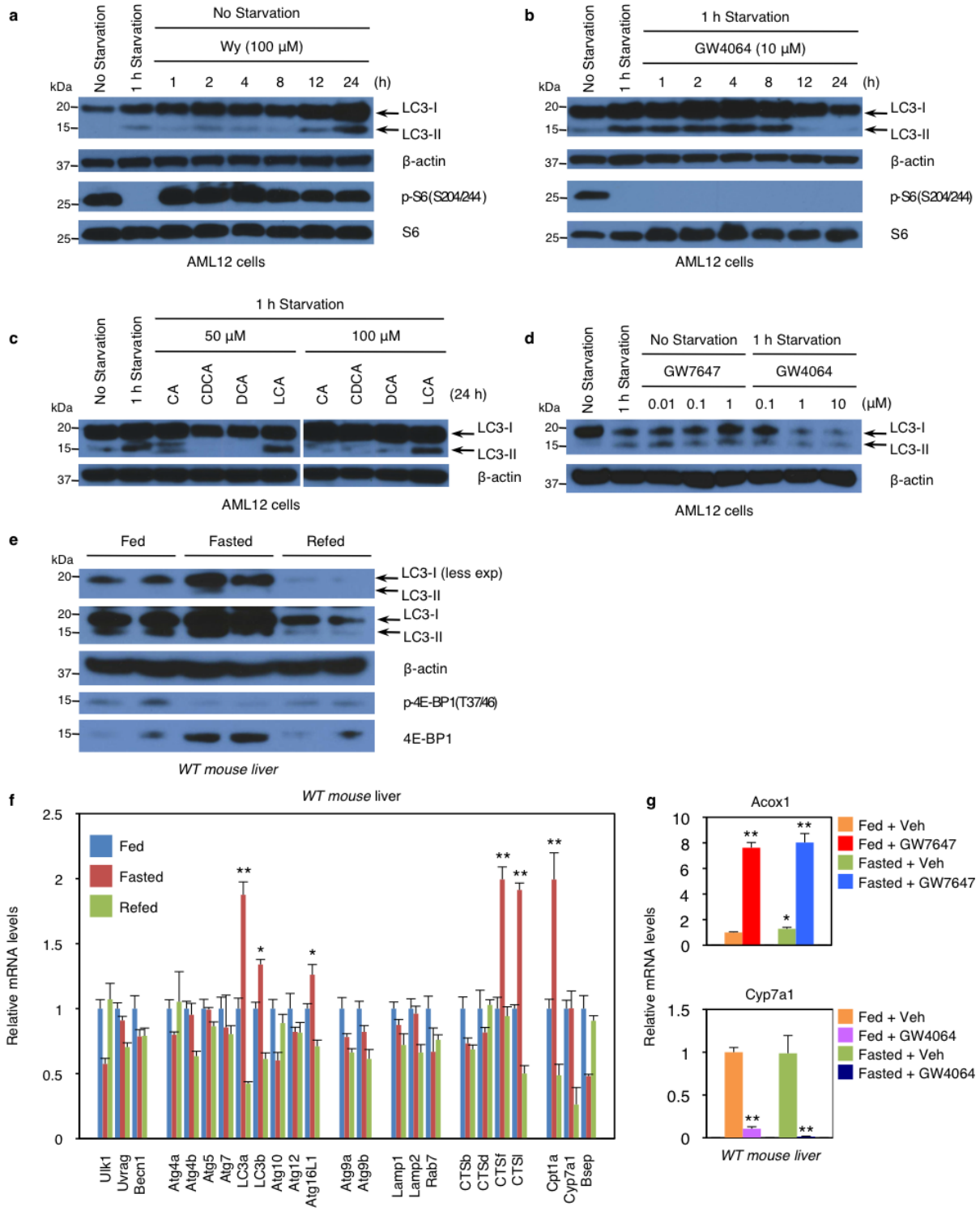

Extended Data Figure 2 | Nutrient availability regulates the expression of autophagy-related genes. **a**, **b**, Biochemical determination of autophagy (LC3 immunoblot; LC3-I and LC3-II denote non-lipidated and phosphatidylethanolamine-conjugated forms of MAP1LC3, respectively) or mTORC1 activity (p-S6(Ser 240/244) immunoblot) in AML12 cells treated for indicated time with 100 μM Wy-14,643 or 10 μM GW4064. GW4064-treated cells were starved in HBSS medium for 1 h. β-actin is a loading control. **c**, Bile acids suppress autophagosome formation. AML12 cells were treated with indicated doses of each bile acid for 24 h, followed by 1-h starvation in HBSS medium. **d**, Immunoblot analysis of LC3-I/II and β-actin in AML12 cells treated with indicated dose of GW7647 or GW4064 for 24 h. GW4064-treated cells were starved in HBSS medium for 1 h. **e**, **f**, Fed *ad libitum*, 24 h fasted, or 24 h refed after 24 h fasting wild-type mice were euthanized to collect livers at 18:00. **e**, Immunoblot analysis of LC3-I/II, β-actin, phosphorylated 4E-BP1 (p-4E-BP1(Thr 37/46)) and total 4E-BP1 in liver samples. Proteins (50 μg) from liver homogenates were separated by SDS–PAGE and probed with the indicated antibodies. β-actin is a loading control. A pooled sample was loaded onto the gel in duplicate ($n = 5$ per group). **f**, Hepatic expression levels of autophagy-related genes, and PPARα and FXR target genes affected by nutrient availability ($n = 5$ per group, $^*P < 0.05$, $^{**}P < 0.01$ versus fed wild-type mice; two-tailed *t*-test). **g**, Hepatic expression levels of PPARα or FXR target gene (*Acox1* and *Cyp7a1*, respectively) were determined by qPCR analysis. Fed or fasted wild-type mice were orally gavaged with vehicle, GW7647 or GW4064 twice a day ($n = 5$ per group, $^*P < 0.05$, $^{**}P < 0.01$ versus fed wild-type mice). Data represent mean ± s.e.m.

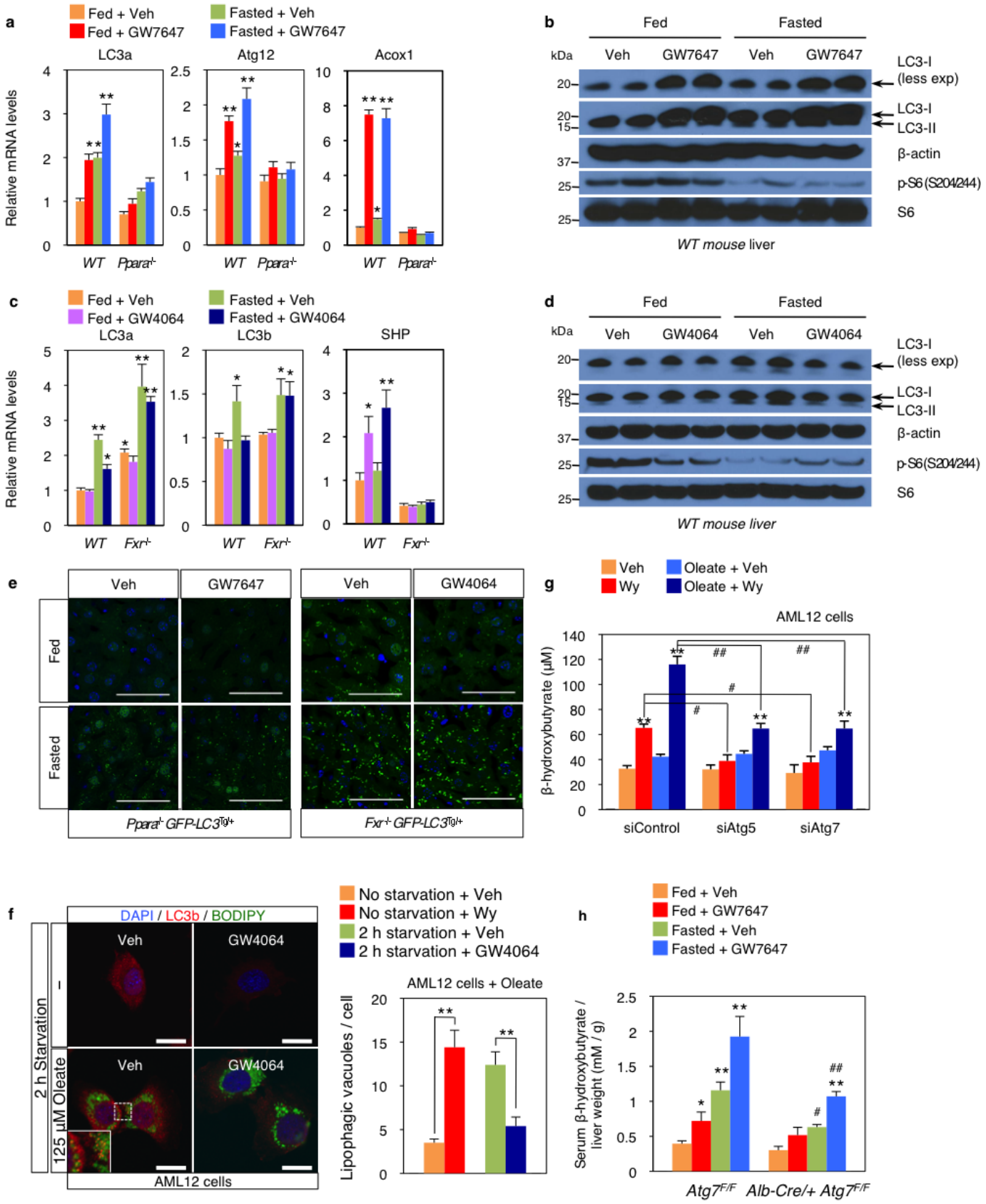

Extended Data Figure 3 | Pharmacological activation of PPARα or FXR in fed or fasted mouse liver. **a**, **c**, Hepatic expression levels of autophagy-related genes (*LC3a*, *LC3b* and *Atg12*), PPARα-target gene (*Acox1*) and FXR-target gene (*SHP*) were determined by qPCR analysis. Fed or fasted wild-type, $Ppara^{-/-}$ or $Fxr^{-/-}$ mice were orally treated with vehicle, GW7647 or GW4064 twice a day ($n = 5$ per group, $^{*}P < 0.05$, $^{**}P < 0.01$ versus fed wild-type mice treated with vehicle). **b**, **d**, Immunoblot analysis of LC3-I/II, β-actin, phosphorylated S6 (p-S6) and total S6 in liver samples. Fed or fasted wild-type mice were orally gavaged with vehicle, GW7647 or GW4064 twice a day. A pooled sample was loaded onto the gel in duplicates ($n = 5$ per group). β-actin is a loading control. **e**, Representative confocal images (out of nine tissue sections per condition) of GFP–LC3 puncta (green: autophagosomes) and DAPI (blue: DNA) staining in livers. Fed or fasted bigenic $Ppara^{-/-}$ *GFP-LC3*$^{Tg/+}$ or $Fxr^{-/-}$ *GFP-LC3*$^{Tg/+}$ mice were orally gavaged with vehicle, GW7647 or GW4064 twice a day. Liver samples were fixed and cryosections were analysed by confocal microscopy. Scale bars, 50 μm. **f**, Co-localization of BODIPY 493/503 (green) with LC3 (red) in AML12 cells treated with vehicle or 1 μM GW4064 for 24 h and simultaneously cultured with or without 125 μM oleate in complete medium. GW4064-treated cells were starved for 2 h. DNA was stained with DAPI (blue). Scale bars, 20 μm. Quantification of lipophagic vacuoles shown in **f** and Fig. 3b. Thirty cells were counted per condition ($^{**}P < 0.01$). **g**, Measuring β-hydroxybutyrate. AML12 cells were transiently transfected with control siRNA (siControl), *Atg5* siRNA (siAtg5) or *Atg7* siRNA (siAtg7) for 24 h followed by indicated drug treatments for 48 h with or without 250 μM oleate (vehicle: 0.1% DMSO, Wy: 10 μM Wy-14,643). Released β-hydroxybutyrate in the medium was determined ($^{**}P < 0.01$ versus siControl treated with vehicle; $^{\#}P < 0.01$ versus siControl treated with Wy-14,643; $^{\#\#}P < 0.01$ versus siControl treated with oleate plus Wy-14,643). **h**, Serum β-hydroxybutyrate were normalized to liver weights. Fed or 24-h fasted control littermates ($Atg7^{F/F}$) and hepatocyte-specific $Atg7^{F/F}$-null (*Alb-Cre*/+ $Atg7^{F/F}$) mice were treated with vehicle or GW7647 twice a day ($n = 4$ per group, $^{*}P < 0.05$, $^{**}P < 0.01$ versus fed $Atg7^{F/F}$ mice treated with vehicle; $^{\#}P < 0.01$ versus fasted $Atg7^{F/F}$ mice treated with vehicle; $^{\#\#}P < 0.01$ versus fasted $Atg7^{F/F}$ mice treated with GW7647). Data are mean ± s.e.m. Statistics by two-tailed *t*-test.

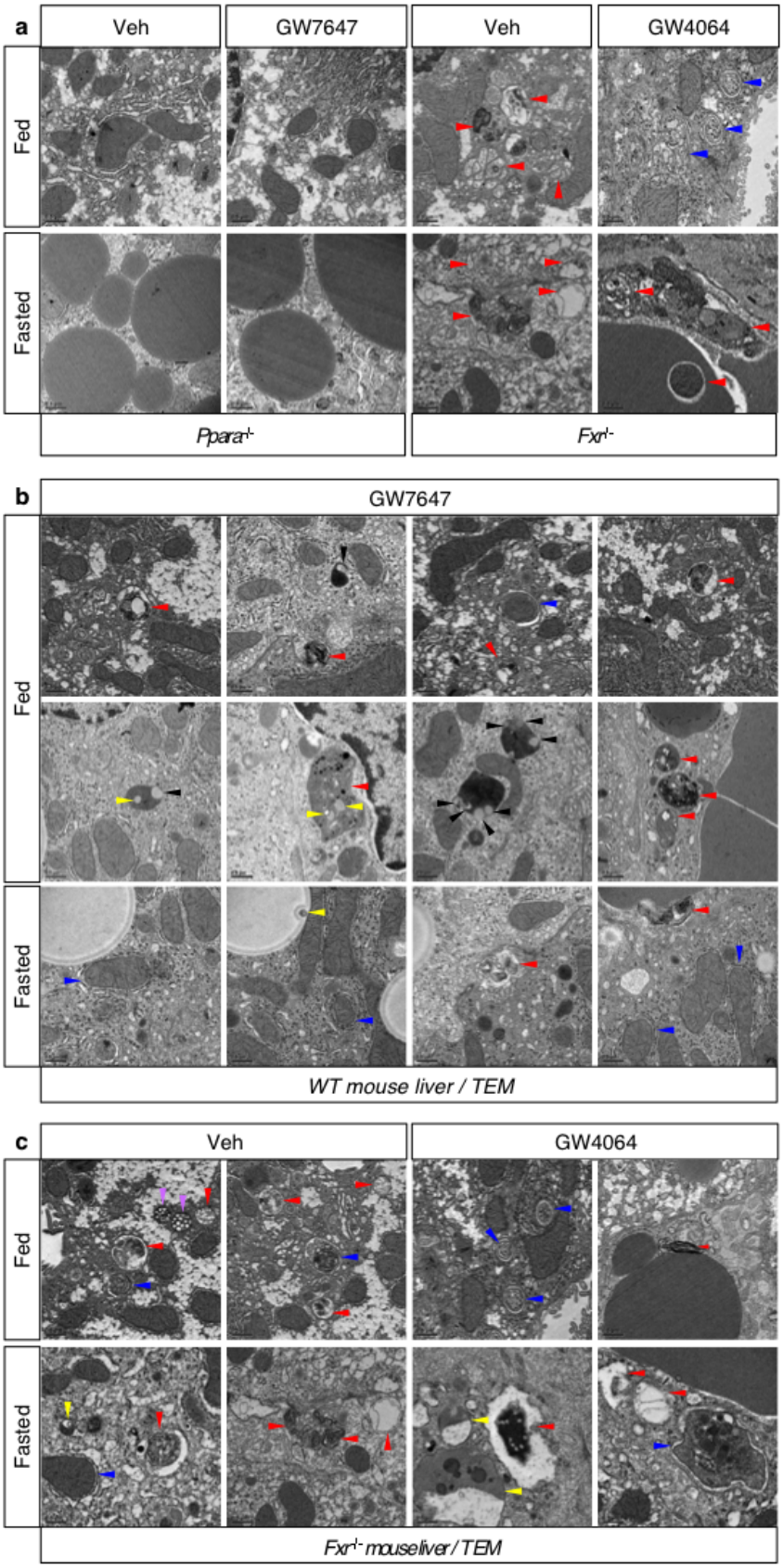

Extended Data Figure 4 | PPARα activation or loss of FXR induces autophagy in liver. Magnification of representative transmission electron micrograph images (out of 30 cells per group) of livers. **a–c**, Fed or fasted wild-type, *Ppara*$^{-/-}$ or *Fxr*$^{-/-}$ mice were orally gavaged with vehicle, GW7647 or GW4064 twice a day. Lipophagy (yellow arrowheads), autophagosomes (blue arrowheads), autolysosomes (red arrowheads), microautophagy (black arrowheads) and multivesicular bodies (purple arrowheads). Scale bars, 0.5 μm.

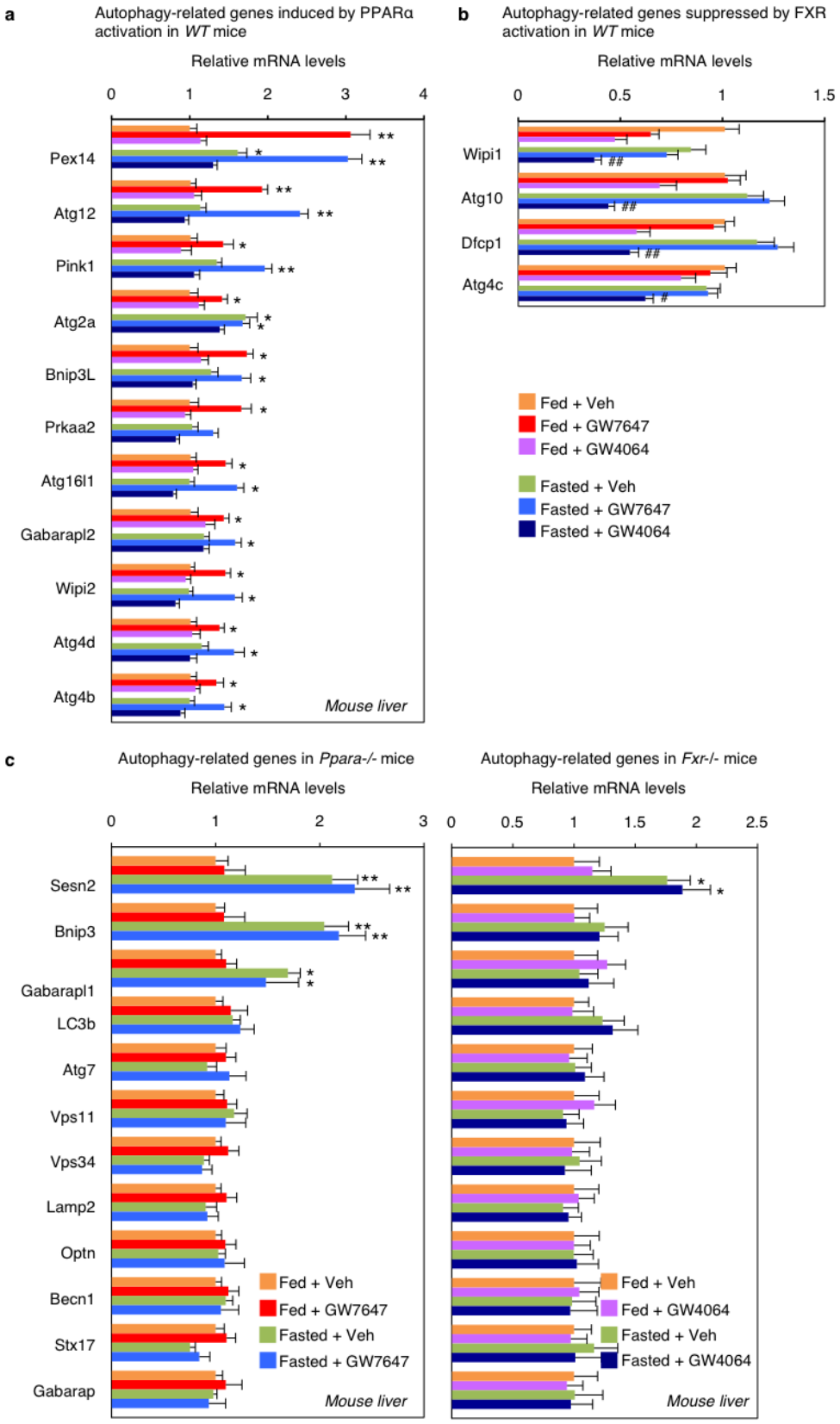

Extended Data Figure 5 | Expression profiles of autophagy-related genes by PPARα or FXR activation in liver. **a**–**c**, Hepatic expression levels of autophagy-related genes were determined by qPCR analysis in wild-type (**a**, **b**), $Ppara^{-/-}$ or $Fxr^{-/-}$ (**c**) mice. Eleven genes in **a** were induced by PPARα activation, but not affected by FXR activation. Four genes in **b** were suppressed by FXR activation, but not affected by PPARα activation (**a** and **b**, $n = 5$ per group, $^{*}P < 0.05$, $^{**}P < 0.01$ versus fed wild-type mice treated with vehicle; $^{\#}P < 0.05$, $^{\#\#}P < 0.01$ versus fasted wild-type mice treated with vehicle). Altered expression levels of 13 genes shown in Fig. 4a were lost in $Ppara^{-/-}$ or $Fxr^{-/-}$ mice in **c** ($n = 5$ per group, $^{*}P < 0.05$, $^{**}P < 0.01$ versus fed $Ppara^{-/-}$ or $Fxr^{-/-}$ mice treated with vehicle). Fed or fasted wild-type, $Ppara^{-/-}$ or $Fxr^{-/-}$ mice were orally gavaged with vehicle, GW7647 or GW4064 twice a day. Data represent mean ± s.e.m. Statistics by two-tailed *t*-test.

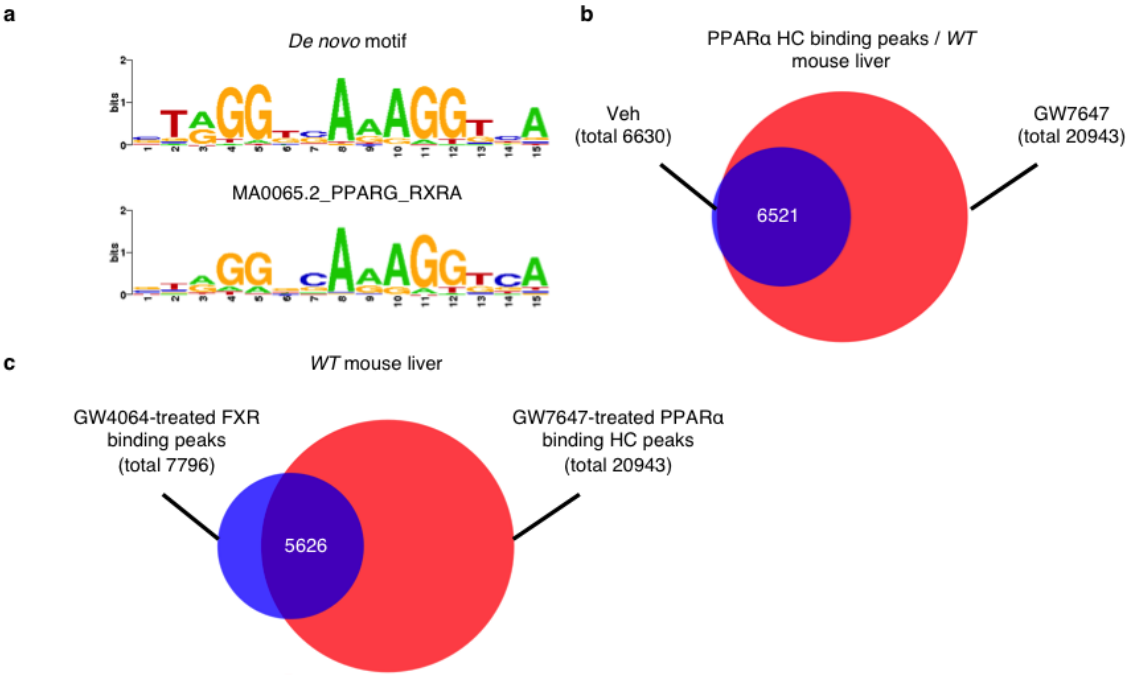

d

Total number of autophagy genes: 230
Total number of genes in mm9: 28661

	PPARα target gene			FXR target gene		
Search range from TSS	5 kb	10 kb	20 kb	5 kb	10 kb	20 kb
Total number of genes with binding peaks	3812	5463	7738	1869	2587	3835
Number of autophagy-related genes with binding peaks	70	91	124	34	46	61
p Value by hypergeometric test	1.1e-11	3.4e-12	7.3e-18	7.4e-6	2.5e-7	9.4e-8

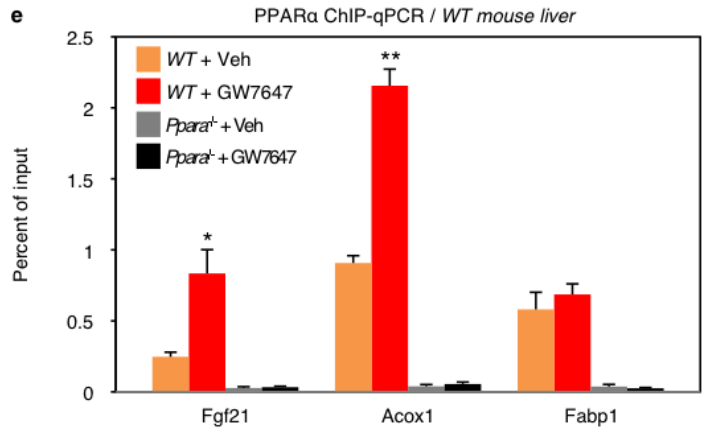

Extended Data Figure 6 | Cistromic analysis of PPARα and FXR in mouse liver. a, *De novo* motif analysis of PPARα-bound genomic regions. Top PPARα peak regions (±150 base pairs (bp) from peak summits, ranked by enrichment fold) were subjected to *de novo* motif discovery by MEME. The best motif discovered by MEME (top, E value $= 4.7 \times 10^{-227}$) highly resembles the PPARγ/RXRA heterodimer binding motif from JASPAR (bottom, ID: MA0065.2) as a direct repeat 1 motif (DR1). **b**, Venn diagram depicting increasing PPARα cistrome upon PPARα agonism *in vivo*. PPARα highly confident (HC) binding peaks: peaks of wild-type mice treated with vehicle or GW7647 subtracted from peaks of *Ppara*$^{-/-}$ mice treated with vehicle or GW7647, respectively. **c**, Venn diagram showing overlapping binding peaks between PPARα ChIP-seq and FXR ChIP-seq from wild-type mice treated with synthetic agonists GW7647 or GW4064. **d**, Autophagy-related genes of PPARα and FXR cistrome. Within 20 kb from the transcription start site (TSS), PPARα ChIP-seq showed that 7,738 genes of total 28,661 genes (mm9) have highly confident peaks in wild-type mice treated with GW7647 (false discovery rate (FDR) < 0.0001, enrichment over *Ppara*$^{-/-}$ > 10), and that 124 genes out of 230 autophagy-related genes (HADb: Human Autophagy Database, http://autophagy.lu/) have at least one PPARα peak. FXR ChIP-seq showed that 3,835 genes have peaks in wild-type mice treated with GW4064, and 61 out of 231 autophagy-related genes have at least one FXR peak. **e**, PPARα ChIP-qPCR for known PPARα target genes ($n = 4$ per group, $^{*}P < 0.05$, $^{**}P < 0.01$ versus fed wild-type mice treated with vehicle; two-tailed t-test). Data represent mean ± s.e.m.

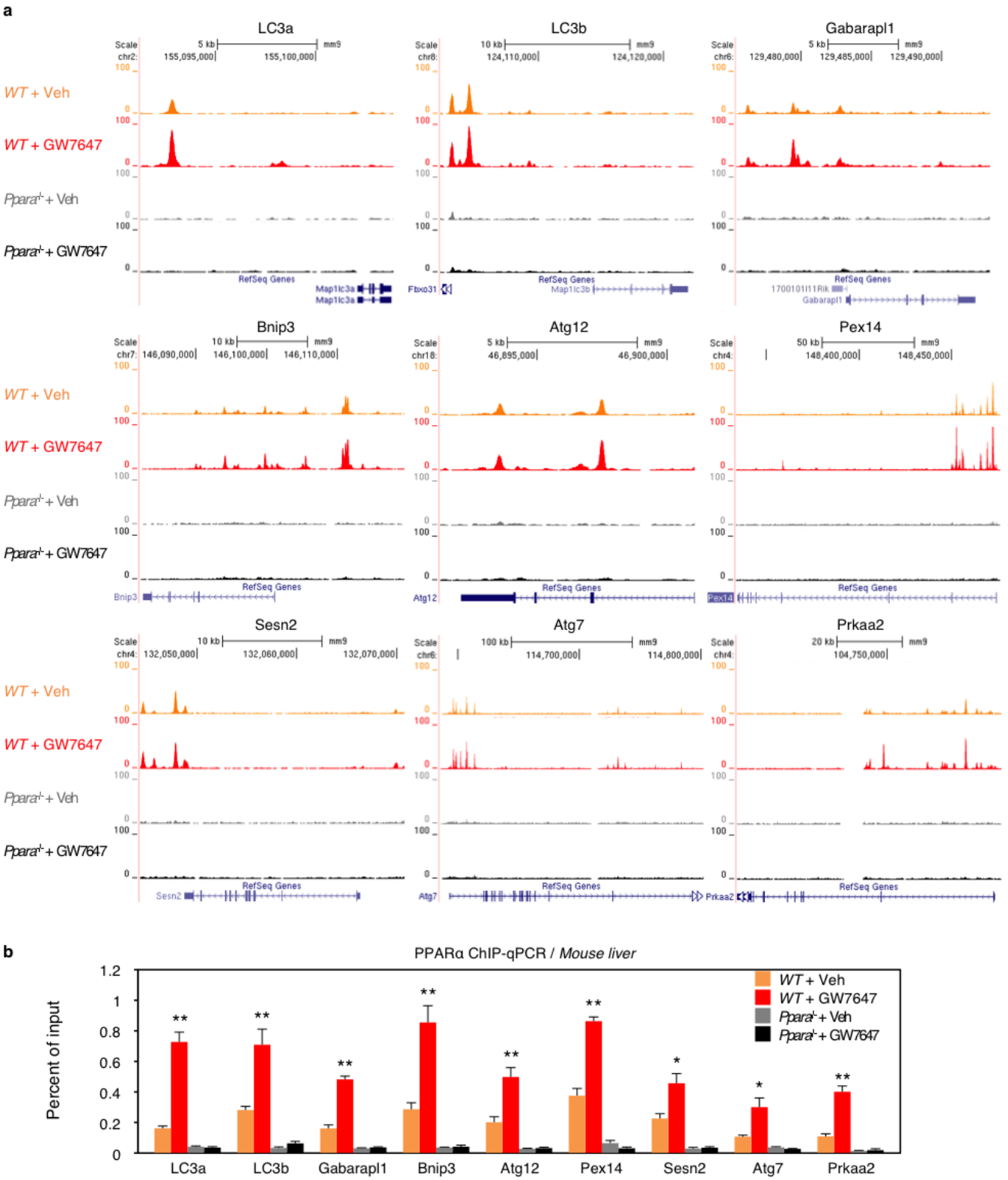

Extended Data Figure 7 | PPARα ChIP-seq profiles at loci of autophagy-related genes. Fed wild-type or *Ppara*$^{-/-}$ mice were orally gavaged with vehicle or GW7647 twice a day. Mouse livers were taken out 6 h after the last injection of drugs to perform PPARα ChIP-seq and ChIP-qPCR. **a**, Representative ChIP-seq reads for PPARα aligned to the autophagy-related genes (*LC3a*, *LC3b*, *Gabarapl1*, *Bnip3*, *Atg12*, *Pex14*, *Sesn2*, *Atg7* and *Prkaa2*). **b**, PPARα ChIP-qPCR for autophagy-related genes shown in **a** ($n = 4$ per group, $^{*}P < 0.05$, $^{**}P < 0.01$ versus fed wild-type mice treated with vehicle; two-tailed *t*-test). Data represent mean ± s.e.m.

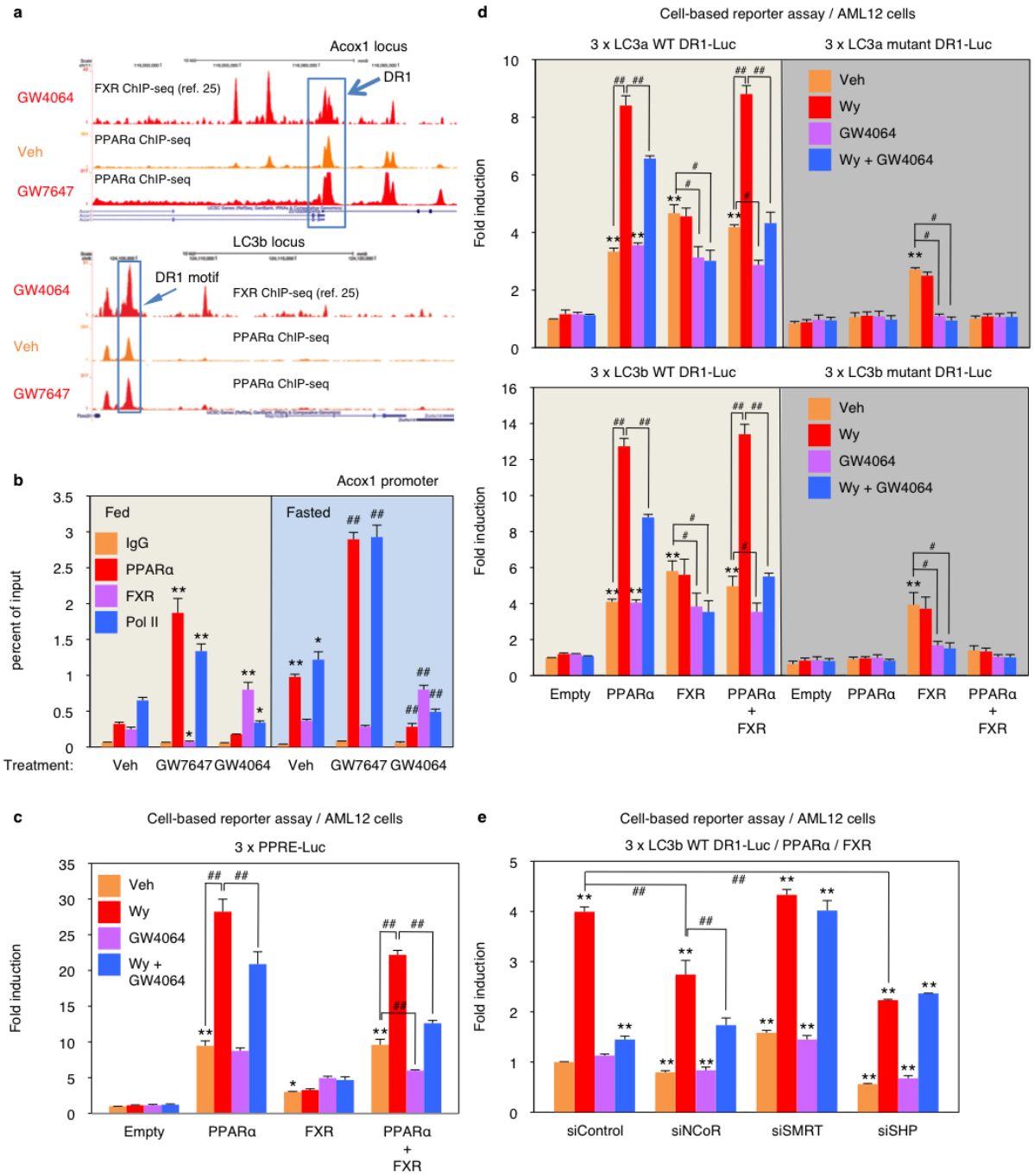

Extended Data Figure 8 | PPARα/FXR genomic competition for DR1 in *Acox1* gene and autophagy-related genes. **a**, Representative ChIP-seq reads for FXR and PPARα aligned to the *Acox1* and *LC3b* genes. The peaks in the box contain DR1 motif. Fed wild-type mice were orally gavaged with vehicle or GW764 twice a day ($n = 4$ per group). **b**, PPARα or FXR ChIP-qPCR in livers. Fed or fasted wild-type mice were orally gavaged with vehicle, GW7647 or GW4064 twice a day ($n = 3$ per group, $^{*}P < 0.05$, $^{**}P < 0.01$ versus fed wild-type mice treated with vehicle; $^{\#\#}P < 0.01$ versus fasted wild-type mice treated with vehicle). **c**, Cell-based luciferase reporter assays. AML12 cells were transiently transfected with a 3×PPRE luciferase reporter construct (3×PPRE-luc) and CMX-β-galactosidase in a combination of expression plasmids of PPARα, FXR or both, followed by drug treatment for 20 h (vehicle: 0.1% DMSO; Wy: 10 μM Wy-14,643; GW4064: 1 μM GW4064). Normalized values (luciferase activity/β-galactosidase activity) of vehicle-treated cells transfected with empty plasmid were set as fold 1 ($^{*}P < 0.05$, $^{**}P < 0.01$ versus empty treated with vehicle; $^{\#\#}P < 0.01$). **d**, Functional role of DR1 motif in the regulatory region of mouse LC3a and LC3b for PPARα or FXR activity. Cell-based luciferase reporter assays were performed in AML12 cells by transiently transfecting three tandem copies of mouse LC3a/LC3b DR1 luciferase reporter construct (3×LC3a/LC3b DR1 WT-luc) or mutated version (3× LC3a/LC3b DR1 mutant-luc) and CMX-β-galactosidase in a combination of expression plasmids of PPARα, FXR or both, followed by drug treatment for 20 h (vehicle: 0.1% DMSO; Wy: 10 μM Wy-14,643; GW4064: 1 μM GW4064). Normalized values (luciferase activity/β-galactosidase activity) of vehicle-treated cells transfected with empty plasmid were set as fold 1 ($^{**}P < 0.01$ versus empty treated with vehicle; $^{\#}P < 0.05$, $^{\#\#}P < 0.01$). **e**, Cell-based luciferase reporter assays were performed in AML12 cells by transiently transfecting siControl, siNCoR, siSMRT or siSHP along with three tandem copies of mouse LC3b DR1 luciferase reporter construct (3×LC3b DR1 WT-luc), expression plasmids of PPARα and FXR, and CMX-β-galactosidase followed by drug treatment for 24 h (vehicle: 0.1% DMSO; Wy: 10 μM Wy-14,643; GW4064: 1 μM GW4064). Normalized values (luciferase activity/β-galactosidase activity) of vehicle-treated cells transfected with siControl were set as fold 1 ($^{**}P < 0.01$ versus siControl treated with vehicle; $^{\#\#}P < 0.01$). Data represent mean ± s.e.m. Statistics by two-tailed *t*-test.

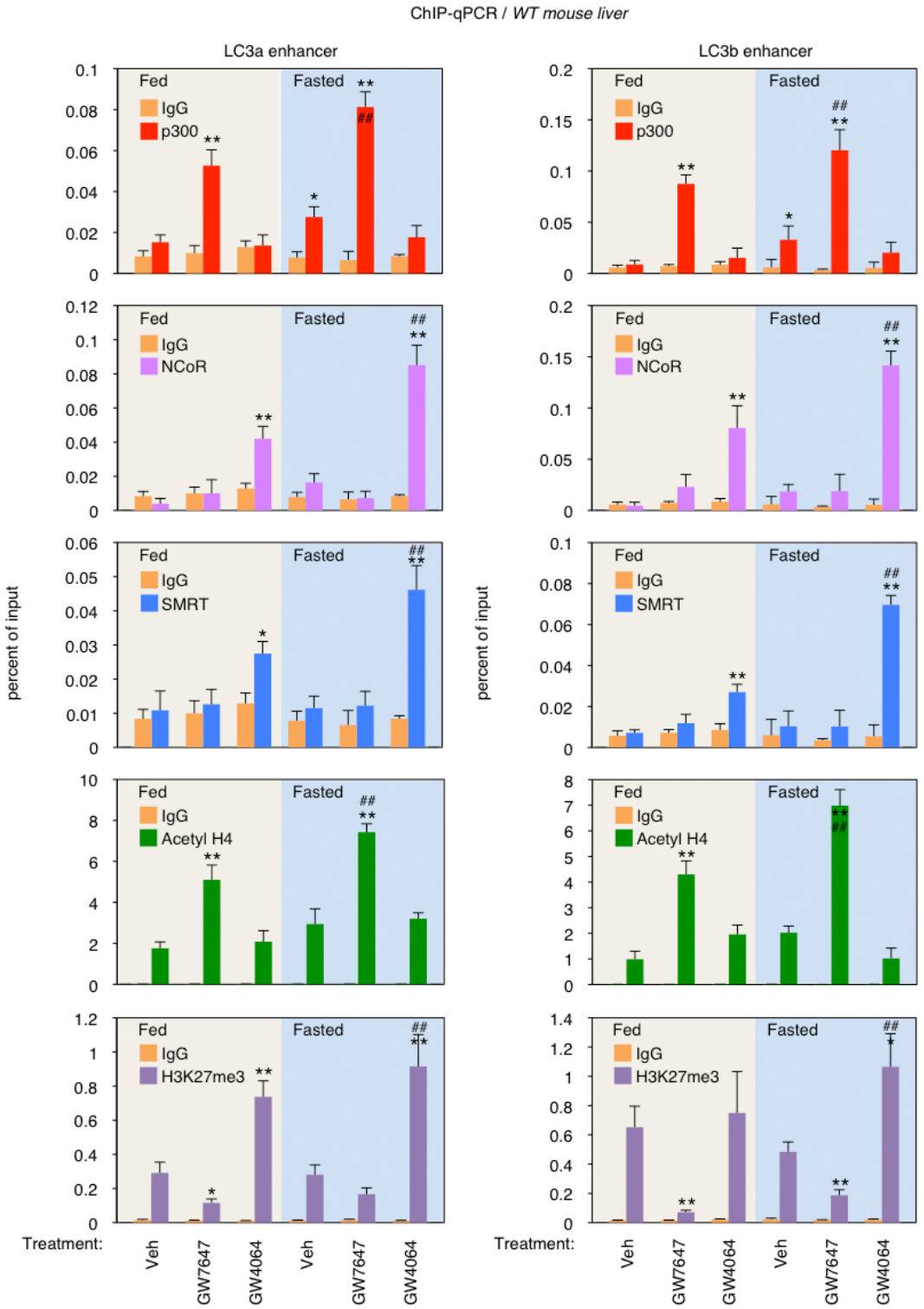

Extended Data Figure 9 | PPARα or FXR activation controls recruitments of co-regulators and epigenetic marks in the enhancer regions of *LC3a* and *LC3b* genes. Fed or fasted wild-type mice were orally gavaged with vehicle, GW7647 or GW4064 twice a day. Hepatic ChIP-qPCR analysis with indicated antibodies (p300, NCoR1, SMRT, acetyl-H4 and H3K27me3) was used to determine recruitments of co-regulators and subsequent alterations of epigenetic marks induced by PPARα/FXR genomic competition for DR1 found in the enhancer region of *LC3a* and *LC3b* genes ($n = 3$ per group, $^{*}P < 0.05$, $^{**}P < 0.01$ versus fed wild-type mice treated with vehicle; $^{\#\#}P < 0.01$ versus fasted wild-type mice treated with vehicle). Data represent mean ± s.e.m. Statistics by two-tailed *t*-test.

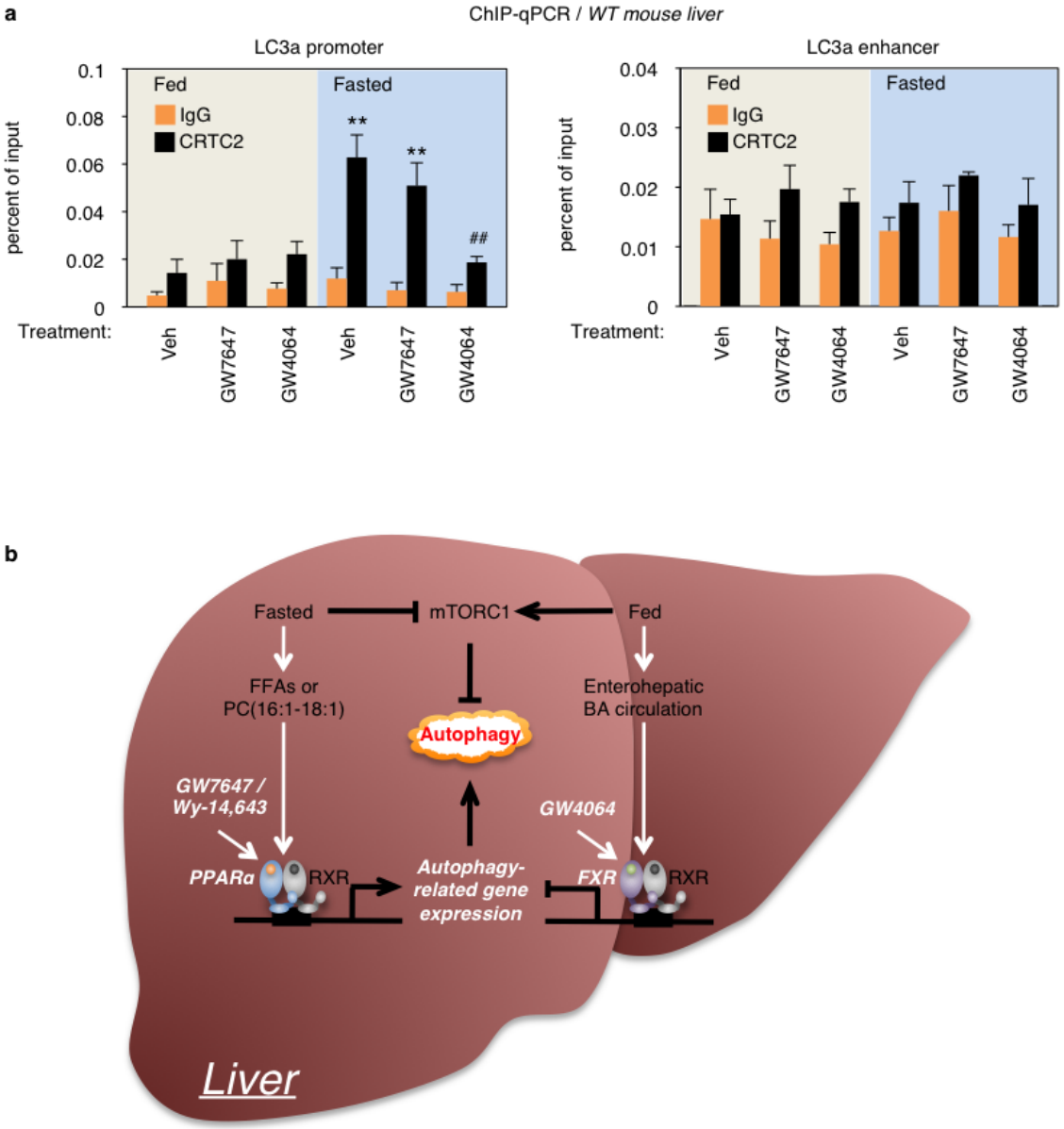

Extended Data Figure 10 | Working model of the coordination of hepatic autophagy by nutrient-sensing nuclear receptors, PPARα and FXR. **a**, Fed or fasted wild-type mice were orally gavaged with vehicle, GW7647 or GW4064 twice a day. Hepatic CRTC2 ChIP-qPCR in the promoter and enhancer region of *LC3a* gene ($n = 3$ per group, $^{**}P < 0.01$ versus fed wild-type mice treated with vehicle; $^{\#\#}P < 0.01$ versus fasted wild-type mice treated with vehicle). Data represent mean ± s.e.m. Statistics by two-tailed *t*-test. **b**, Proposed model depicting transcriptionally activating or suppressive nutrient-sensing nuclear receptors, PPARα or FXR, respectively, which coordinate autophagy in liver. Activated PPARα or FXR compete with each other for binding to response elements found in autophagy-related genes.